Novel phases and reentrant melting of two-dimensional colloidal crystals

Leo Radzihovsky,[1] Erwin Frey,[2] and David R. Nelson[2]
[1]*Department of Physics, University of Colorado, Boulder, Colorado 80309*
[2]*Department of Physics, Harvard University, Cambridge, Massachusetts 02138*
(Received 13 August 2000; published 27 February 2001)

We investigate two-dimensional (2D) melting in the presence of a one-dimensional (1D) periodic potential as, for example, realized in recent experiments on 2D colloids subjected to two interfering laser beams. The topology of the phase diagram is found to depend primarily on two factors: the relative orientation of the 2D crystal and the periodic potential troughs, which selects a set of Bragg planes running parallel to the troughs, and the commensurability ratio $p=a'/d$ of the spacing a' between these Bragg planes to the period d of the periodic potential. The complexity of the phase diagram increases with the magnitude of the commensurabilty ratio p. Rich phase diagrams, with ''modulated liquid,'' ''floating,'' and ''locked floating'' solid and smectic phases are found. Phase transitions between these phases fall into two broad universality classes, roughening and melting, driven by the proliferation of discommensuration walls and dislocations, respectively. We discuss correlation functions and the static structure factor in these phases, and make detailed predictions about the universal features close to the phase boundaries. We predict that for charged systems with highly screened short-range interactions, these melting transitions are generically reentrant as a function of the strength of the periodic potential, a prediction that is in accord with recent 2D colloid experiments. Implications of our results for future experiments are also discussed.

DOI: 10.1103/PhysRevE.63.031503 PACS number(s): 68.35.Rh, 82.70.Dd, 61.72.Lk, 64.70.Dv

I. INTRODUCTION

A. Motivation and background

Two-dimensional (2D) melting and mathematically related systems, such as, for example normal-to-superfluid and planar paramagnet-to-ferromagnet transitions in films (described by the 2D XY model) are striking examples of the increased importance of thermal fluctuations in low-dimensional systems [1,2]. In contrast to their bulk, three- (and higher-) dimensional analogs, where, typically, fluctuations lead only to *quantitative* modifications of mean-field predictions (e.g., change values of critical exponents), here the effects are *qualitative* and drastic. Located exactly at the lower-critical dimension ($d_{lc}=2$), below which the distinction between the high and low temperature phases is erased by fluctuations, two-dimensional melting can proceed via a subtle, two-stage, *continuous* transition, driven by an unbinding of topological defects (dislocations and disclinations). This mechanism, made possible by strong thermal fluctuations, therefore provides an alternative route to a direct first-order melting, argued by Landau's mean-field analysis [3] to be the *exclusive* scenario.

Despite its long history, dating back to the work of Kosterlitz and Thouless [4], Halperin and Nelson [5], and Young [6] (KTHNY) (which in turn built on a large body of ideas dating back to Landau and Peierls [7]), interest in 2D melting and related problems persists. On the theoretical side this is due, in part, to the fact that the theory of 2D melting is an unusual example of a nontrivial and quite exotic critical point that lends itself to an asymptotically *exact* description. Furthermore, the KTHNY class of transitions (2D melting and related disordering of a 2D XY model) provides a rare example of thermodynamically sharp phase transitions between phases, both of which lack long-range order [8].

Although evidence of defect driven phase transitions appeared in numerous experiments on liquid crystals [9] and Langmuir-Blodgett films [10], finding simple model systems which exhibit these phenomena in experiments or simulations has proven to be more controversial. Some system parameters appear to fall into the range in which it is discontinuous melting that converts a solid directly into a liquid. However, it appears that two-stage continuous melting was recently experimentally observed by Murray *et al.* [11] and Zahn *et al.* [12] in beautiful melting experiments on two-dimensional colloids confined between smooth glass plates and superparamagnetic colloidal systems, respectively. In these experiments, an orientationally quasi-long-range ordered but translationally disordered hexatic phase [5] was observed. This phase, intermediate but thermodynamically distinct from the 2D solid and isotropic liquid, is an important signature of defect driven two-stage melting. In these two-dimensional colloids, particle positions and the associated topological defects can be directly imaged via digital video microscopy, allowing precise quantitative tests of the theory. Colloids are thus ideal experimental model systems to explore the details of two-dimensional melting and related phenomena, many of which are the focus of the theory presented here [13].

Soon after the initial development of the theory of two-dimensional melting, theoretical efforts turned toward studies of the effects of a substrate, an important ingredient in many physical systems. These studies [14,15] uncovered a rich phenomenology stemming from the interplay between the underlying periodic substrate and a quasi-long-range ordered solid film interacting with it. While many experiments have been undertaken, with a krypton film on a graphite substrate (see, e.g., Ref. [15] for a review) being one of the best studied, these systems are far from ideal in exploring this rich phenomenology, because of the lack of substrate

tunability; in these systems it is difficult to change the substrate period, dimensionality, and pinning strength.

A series of pioneering experiments by Chowdhury, Ackerson, and Clark [16] constituted an important new development. In these studies strongly interacting colloidal particles, confined to two dimensions, were subjected to a one-dimensional periodic potential, induced by the interference fringes from two laser beams crossed in the sample. The light-induced polarization in these micron-size dielectric particles interacts with the laser electric field, leading to a radiation pressure force [17] directed toward the regions of high laser intensity, the antinodes' maxima in the laser standing wave pattern.

One of many interesting phenomena discovered by Chowdhury *et al.* is the fixed-temperature freezing transition driven by increasing the strength of the laser potential, dubbed ''light induced freezing'' (LIF). Qualitatively, LIF is due to the suppression of thermal fluctuations of the colloidal particles transverse to the imposed periodic pinning laser potential. This intuition is also supported by a more quantitative analysis based on Landau's free energy expansion in the translational order parameters (density Fourier modes) $\rho_{\mathbf{G}_i}$, with the $\{\mathbf{G}_i\}$'s the three smallest reciprocal lattice vectors of a triangular lattice. In the simplest geometry, with e.g., $\mathbf{G}_1$ commensurate with the laser potential, $\langle \rho_{\mathbf{G}_1} \rangle$ is trivially induced by the potential even in the liquid phase. Such a finite $\langle \rho_{\mathbf{G}_1} \rangle$ then converts Landau's cubic coupling $\rho_{\mathbf{G}_1}\rho_{\mathbf{G}_2}\rho_{\mathbf{G}_3}$, (which, in mean-field theory, is responsible for melting always being first order) into a simple upward shift in the melting temperature for the only remaining critical mode $\psi \equiv \rho_{\mathbf{G}_2} - \rho_{\mathbf{G}_3}$. Not surprisingly, the resulting Landau expansion contains only even powers of this complex order parameter ψ, which therefore generically orders via a *continuous* transition in the *XY* universality class. Hence, within the mean-field description discussed by Chowdhury *et al.* [16], one expects to reach a tricritical point upon increasing the light intensity, beyond which the LIF transition becomes continuous.

However, because of the dominant role of thermal fluctuations in two-dimensional systems, such ''soft-spin'' Landau expansions in order parameter amplitudes (and the related density functional theories [18]) will have difficulties in capturing the subtleties of the continuous topological phase transitions possible in these two-dimensional systems. Unfortunately, results from Monte Carlo simulations are inconclusive. Although earlier simulations [19] claimed to have found a tricritical point at intermediate laser intensities, consistent with density functional theory, recent studies from the same laboratory [20] refuted these results. These difficulties are perhaps unsurprising, given that even much larger scale simulations have, so far, failed to completely resolve the nature of 2D melting, even *without* a periodic external potential [21].

An alternative (but complementary and in principle equivalent) ''hard-spin'' defect description (with order parameter amplitude fluctuations represented by defect cores), extended to include a one-dimensional periodic pinning potential may be necessary to correctly capture the rich phenomenology of the early experiments by Chowdhury *et al.* [16] and recent ones by Wei *et al.* [22] and others [23]. Developing such a theoretical framework and exploring its details to interpret these experiments is the goal of the work presented here.

Our interest in this problem was stimulated by the experiments of Wei *et al.* [22], which extended the light-induced melting experiments to higher laser intensities than those studied in Ref. [16]. One other notable difference is that in contrast to the strong long-range interaction of unscreened charged colloids in highly deionized solution [16], in Wei *et al.*'s experiments colloidal particles were interacting via a short-ranged Debye potential, with ions in the solution screening the long-ranged Coulomb interaction. In addition to the light-induced freezing, observed at low light intensities, the authors of Ref. [22] discovered a *reentrant* melting phenomenon, ''light-induced melting'' (LIM), driven by the increased strength of the laser-induced one-dimensional periodic potential. As discussed below, this fascinating reentrance phenomenon *generically* emerges from our theoretical analysis in the limit of a short Debye screening length.

The goal of this paper is to investigate two-dimensional melting in the presence of a one-dimensional periodic potential, and to answer many basic questions stimulated by these recent experiments. What is the nature of such melting transition, if not preempted (as it can always be) by the first-order transition? More generally, how is the standard phase diagram for 2D melting on a homogeneous substrate (which includes the 2D crystal, hexatic and liquid phases) modified by the periodic laser potential? Which of the phases survive the light field and what new ones emerge in its presence? The answers to these and many other questions, provided below, lead to results consistent with experimental observations, and have many testable consequences for possible future experiments.

B. Summary of the results

Even in a liquid phase at high temperatures laser interference fringes, which we choose to run along the *x* axis, induce a periodic density modulation in the colloidal liquid. As a consequence the static structure function $S(\mathbf{q})$ displays Bragg peaks at $\mathbf{K}_n \equiv n(2\pi/d)\hat{\mathbf{y}}$, the integer multiples ($n \in \mathcal{Z}$) of the reciprocal lattice vector $\mathbf{K} = (2\pi/d)\hat{\mathbf{y}}$ of the imposed one-dimensional periodic potential with a trough spacing d [24]. The liquid phase density exhibits a *finite* linear response to such a periodic perturbation with amplitude U_K, which is proportional to the input laser intensity I_{in}. This is consistent with the observations of Chowdhury *et al.* [16], who found the scattered laser intensity I_{out}, at these directly induced Bragg peaks, to scale as a cube of the input laser power I_{in} [25]. These explicitly induced features of the modulated liquid persist throughout the phase diagram, with the additional structure emerging as a result of numerous *spontaneous* symmetry breakings, which we discuss below.

The laser-induced periodic potential also *explicitly* breaks continuous 2D rotational symmetry down to $\mathcal{Z}_2$ symmetry (rotations by π). Consequently, the one-dimensional periodic potential induces nematic, square, hexatic, and higher orientational harmonics long-range orders, respectively,

characterized by a $2n$-atic bond orientational order parameter $\psi_{2n}=\langle e^{i2n\theta(\mathbf{r})}\rangle$, which, independent of any other details, are nonzero throughout the phase diagram. Therefore, in particular, the laser potential eliminates the continuous transition from an isotropic liquid phase to a hexatic liquid phase, expected in two-dimensional liquids in the absence of an external potential [5]. This situation is analogous to a ferromagnet in a magnetic field, where the qualitative distinction between paramagnetic and ferromagnetic phases is erased by the external magnetic field, with both phases displaying a finite induced magnetization.

Since the hexatic orientational order is *explicitly* induced by the laser potential, it must vanish as the laser field is tuned to zero. Analogously to a power-law vanishing of the magnetization with an external magnetic field in a ferromagnet at its critical point, we predict that at low input light intensities $I_{\rm in}$, the orientational order parameter, vanishes as a *universal* power of $I_{\rm in}$,

$$\psi_6 \sim I_{\rm in}^{1/\delta_{\psi_6}}, \tag{1.1}$$

with $1/\delta_{\psi_6}=6$ [26] in the liquid phase and

$$1/\delta_{\psi_6}=\frac{6\,\overline{\eta}_6}{4-\overline{\eta}_6} \tag{1.2}$$

in the hexatic phase, where $\overline{\eta}_6$ is the exponent describing the algebraic decay of bond orientational order in the absence of the laser-induced periodic potential [5]. We expect ψ_6 to approach a nonzero $I_{\rm in}$-independent constant in the solid phase, consistent with the *spontaneous* long-range hexatic order of the 2D crystal, even in the absence of a periodic potential.

All other details of the phase diagram and the properties of the phases for our system depend strongly on the level of commensurability between the two-dimensional colloidal crystal, in the absence of the laser field, and the one-dimensional periodic potential that it induces. This in turn is determined by two ingredients: (i) the orientation of the triangular colloidal lattice relative to that of the periodic potential troughs, which selects a set of Bragg planes that run parallel to the troughs; and (ii) the commensurability ratio of the spacing a' between these Bragg planes to the period d of the laser potential, defined by $p\equiv a'/d$. In this paper we will primarily focus on the commensurate case defined by $p\in\mathcal{Z}$, and defer the rich phenomenology of the incommensurate case and the commensurate-incommensurate transitions to a later publication [27].

For these commensurate densities, independent of the order of commensurability p, at the lowest temperatures we always find that our system freezes into an interesting type of a crystal, which we call a ''locked floating solid'' (LFS) phase. This phase derives its apparently contradictory name from its highly anisotropic properties: while the solid is pinned transversely to the troughs of the periodic potential, executing only massive optical phonon-like excitations in that direction, it is able to slide freely along the potential minima with acoustic phonon excitations within the troughs.

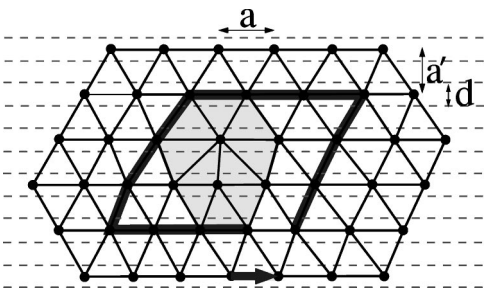

FIG. 1. Triangular lattice with lattice constant a subject to a periodic potential (maxima indicated by dashed lines) for $pd=a'$, with $a'=\sqrt{3}a/2$ and $p=2$. Also shown is the low energy dislocation with Burgers vector **b** parallel to the corrugation of the external potential.

Upon integrating out the massive u_y modes and using standard renormalization group methods [5] to eliminate bound dislocation pairs in the LFS phase, we are left with a free energy with temperature and potential strength dependent *effective* elastic constants:

$$H_{\rm LFS}=\frac{1}{2}\int d^2r\{K_{\rm eff}(\partial_x u_x)^2+\mu_{\rm eff}(\partial_y u_x)^2\}. \tag{1.3}$$

The structure function of a LFS is quite unusual. Like the high temperature modulated liquid discussed above, the LFS displays a set of delta-function Bragg peaks (reduced by the Debye-Waller factor) located at the multiples of the laser potential reciprocal lattice vector $\mathbf{K}=(2\pi/d)\hat{\mathbf{y}}$, which coexist with other *spontaneously* induced Bragg and quasi-Bragg peaks.

The more detailed properties of the LFS and other phases exhibited by our system, strongly depend on the choice of the infinite set of colloidal crystal orientations relative to the light interference fringes. While we will explore these numerous possibilities in their full generality in the main body of the paper, in this subsection we summarize our results only for the simplest orientation studied in the experiments of Refs. [16,22], in which the periodic potential troughs run parallel to the *primary* Bragg planes [28].

Experimentally, we expect our system to display a considerable amount of irreversibility, with the choice of the relative orientation highly dependent on the way the system is taken into the crystal state: if the laser potential is turned on in the liquid phase (field cooled), the crystal will freeze into the lowest energy orientation consistent with the imposed colloidal density (or the chemical potential) and laser fringe spacing [29]; in contrast, in zero-laser-field cooling experiments, an already formed crystal may be unable to reorient significantly, and will therefore lock into a metastable orientation, determined by the plane of the two interfering laser beams.

Once we focus on the primary orientation, illustrated for $p=2$ in Fig. 1, the phenomenology of our system is completely determined by the integer commensurability ratio p. As we will show, for commensurate densities, our system admits three phase diagram topologies, corresponding to the

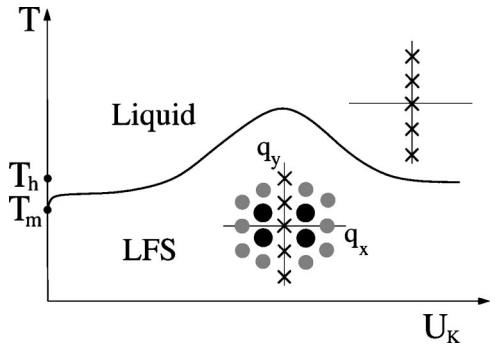

FIG. 2. Schematic phase diagram for a primary commensurate orientation with commensurability ratio $p=1$. T_h indicates the transition temperature from the hexatic to the isotropic liquid phase at $U_K=0$. *Insets:* Schematic structure functions in the various phases. The $\times$'s indicate delta-function Bragg peaks, and the shaded circles algebraic peaks.

three ranges of the values of p: (i) $p=1$ [30], (ii) $1<p\leqslant p_c$, and (iii) $p>p_c$, with the critical value of $p_c\approx 3.7$ for the primary orientation.

1. Commensurability ratio $p=1$

For $p=1$ [30], we find the phase behavior of the 2D colloidal system as summarized by the phase diagram illustrated in Fig. 2.

Because the sharp distinction between the hexatic and isotropic liquid phases is absent in the presence of a periodic potential, this phase diagram contains only two thermodynamically distinct phases at finite U_K: the modulated liquid phase and the simplest $p=1$ ''locked floating solid'' phase. We can estimate the order of magnitude of the transition temperature between the LFS and liquid phases in terms of microscopic elastic constants [similar to those appearing in Eq. (1.3)] as follows: In the limit of a strong laser potential the particles are confined to a parallel array of equally spaced 1D channels of spacing d, illustrated in Fig. 3. If $u_n(x)$ is the particle displacement field along the nth channel, we can write the energy of these weakly coupled one-dimensional rows of particles as

$$H=d\sum_n \int dx\left\{\frac{1}{2}K\left(\frac{du_n}{dx}\right)^2 - \mu\left(\frac{a}{2\pi d}\right)^2\cos\left[\frac{2\pi}{a}[u_{n+1}(x)-u_n(x)]\right]\right\}, \quad (1.4)$$

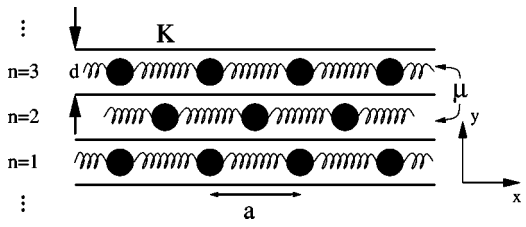

FIG. 3. Colloidal particles in channels, labeled by n, with intrachannel compressional modulus K and interchannel shear coupling μ.

where K is the bare compressional elastic modulus within each channel, and μ is the microscopic coupling between the channels determining the shear modulus of the 2D system [31]. At high temperatures or weak microscopic coupling μ, the colloid decomposes into an orientationally ordered two-dimensional liquid of decoupled one-dimensional channels. At temperature T, the phonon fluctuations within a channel then grow according to

$$\langle|u_n(x)-u_n(0)|^2\rangle=\frac{k_BT}{dK}x, \quad (1.5)$$

as can be seen from the equipartition theorem. Upon choosing x such that the root mean square phonon fluctuations are equal to the intrachannel particle spacing a, we determine a translational correlation length $\xi_T(T)$, which diverges at low temperatures:

$$\xi_T(T)=\frac{Kd}{k_BT}a^2. \quad (1.6)$$

The channels will couple to form a coherent two-dimensional LFS phase when the effective coupling $d\xi_T(T)\mu(a/2\pi d)^2$ between correlated 1D regions of size $\xi_T(T)$ surpasses the thermal energy k_BT which decorrelates the 1D channels. We associate this characteristic temperature with the melting temperature T_m of the LFS phase, which is therefore given by

$$k_BT_m=\text{const}\times a^2\sqrt{\mu K}. \quad (1.7)$$

A similar argument leads to the estimate for freezing into the three-dimensional locked floating solid phases discussed by Carraro [32] for rare gas atoms adsorbed into bundles of carbon nanotubes. As we describe in Appendix A, in terms of the weakly coupled model [Eq. (1.4)], freezing into a LFS takes place at a strong coupling μ, and therefore does not allow a rigorous renormalization group treatment of the transition. Nevertheless an approximate variational treatment is possible, and is presented in Appendix A.

Instead, here we take an alternative route to the study of the LFS melting and other transitions by working within a continuum elastic model [Eq. (1.3)], which is equivalent to the strong coupling (between the channels) limit of the discrete model in Eq. (1.4). Such an approach allows a more refined and asymptotically exact renormalization group analysis (presented below), within which we find that for $p=1$ the melting of the LFS phase is in the universality class of the XY model, and is driven by unbinding of dislocation pairs with Burgers vectors $\mathbf{b}=a\hat{\mathbf{x}}$ along the troughs of the periodic potential. Consequently, in contrast to the conventional 2D melting transition, at the melting temperature T_m, we predict a *universal* ratio of the jump in the geometric mean of the long wavelength effective shear and bulk moduli, $\mu_{\text{eff}}(T_m^-)$ and $K_{\text{eff}}(T_m^-)$ (describing the elasticity of the LFS phase) to T_m:

$$\frac{\sqrt{K_{\text{eff}}(T_m^-)\mu_{\text{eff}}(T_m^-)}}{k_BT_m}=\frac{8\pi}{|\mathbf{b}|^2}. \quad (1.8)$$

This is in agreement, up to constants of order 1, with the rough estimate of the melting temperature [Eq. (1.7)] sketched above, and with the variational method presented in Appendix A. The most striking feature of the $p=1$ LFS melting phase transition is the shape of the phase boundary $T_m(U_K)$, whose universal features guarantee a generically reentrant melting, under conditions such as the experiments of Wei *et al.* [22]. At low light intensities, i.e., small U_K, we find that the melting curve has a universal, cusp shape,

$$T_m(U_K) \sim T_m(0) + [\ln(k_B T_m/U_K)]^{-1/\bar{\nu}}, \tag{1.9}$$

with $\bar{\nu} \approx 0.36963$. On the other hand, for large U_K, i.e., for $k_B T_m(U_K)/U_K \ll 1$, we find that for short-range particle interactions ($\kappa a \gtrsim 5.8$), $T_m(U_K)$ generically *increases* with decreasing amplitude U_K of the periodic modulation, according to

$$T_m(U_K) = T_m^{\infty}\left\{1 + \frac{5[(\kappa a)^2 - 31]}{64\pi^2}\left(1 + \frac{13}{3\kappa a}\right)\frac{k_B T_m^{\infty}}{p^2 U_K}\right\} \tag{1.10}$$

thus implying reentrant melting for a band of temperatures as a function of potential strength (see Fig. 2). In Eq. (1.10) above, κ is the inverse of the Debye screening length, tunable by adjusting the solution salt concentration, and $T_m^{\infty} \equiv T_m(U_K \to \infty)$, which, for the system studied in Ref. [22], we estimate to be approximately $1.3 T_m(U_K = 0)$.

The structure function for the $p=1$ LFS phase, illustrated in Fig. 2, is also quite unusual. In addition to the set of Bragg peaks, directly induced by the laser field, $S(\mathbf{q})$ also displays an independent set of *quasi*-Bragg peaks at the off-q_y-axis reciprocal lattice vectors $\mathbf{G}$ [5],

$$S(\mathbf{q}) \sim \frac{1}{|\mathbf{q} - \mathbf{G}|^{2-\eta_{\mathbf{G}}}}, \tag{1.11}$$

which distinguishes the LFS from the modulated liquid state. The corresponding density-density correlation function $C_{\mathbf{G}}(\mathbf{r}) = \langle \rho_{\mathbf{G}}(\mathbf{r}) \rho_{\mathbf{G}}^*(0) \rangle$, for reciprocal lattice vectors with $G_x \neq 0$ shows a power-law decay

$$C_{\mathbf{G}}(\mathbf{r}) \sim \left| \left(\frac{\mu_{\rm eff}}{K_{\rm eff}}\right)^{1/2} x^2 + \left(\frac{K_{\rm eff}}{\mu_{\rm eff}}\right)^{1/2} y^2 \right|^{-\eta_{\mathbf{G}}/2}, \tag{1.12}$$

where $\mu_{\rm eff}$ and $K_{\rm eff}$ are the effective shear and bulk elastic moduli in Eq. (1.3) for the deformations along the troughs (x axis) of the periodic potential. The exponent $\eta_{\mathbf{G}}$ depends on the relative orientation of the colloidal crystal and the troughs. Unlike conventional 2D melting [5], it is *universal* at the melting transition, and is given by

$$\eta_{\mathbf{G}}^* \equiv \eta_{\mathbf{G}}(T_m^-) = (\mathbf{G} \cdot \mathbf{b}/4\pi)^2, \tag{1.13}$$

where $\mathbf{b}$ is the smallest allowed Burgers vector in the trough direction. For the primary orientation, illustrated in Fig. 1, with $b = a$, the exponent characterizing the algebraic order in the off-axis peaks (see Fig. 2) closest to the q_y axis is $\eta_{\mathbf{G}}^* = 1/4$; for the next row of peaks, with $G_x = 4\pi/a$, we find $\eta_{\mathbf{G}}^* = 1$, consistent with the algebraic decay observed in Ref. [22] (for a more detailed discussion, see Sec. VII).

Our analysis also makes *exact* predictions for the structure function peak amplitudes in the limit of low laser intensity. Similar to the hexatic orientational order parameter ψ_6 [Eq. (1.1)], the translational order parameter, defined by $M_{\mathbf{K}_n} \equiv \langle \rho_{\mathbf{K}_n} \rangle$, is induced by the periodic potential throughout the phase diagram. However, in contrast to the liquid phase, where it vanishes linearly with U_K, in the crystal phase, for $T < T_m(0)$, we find

$$M_{\mathbf{K}_n} \sim |U_K|^{1/\delta_M}, \tag{1.14}$$

with δ_M defined in analogy with the critical exponent at a ferromagnetic critical point,

$$1/\delta_M = \frac{\bar{\eta}_{\mathbf{K}_n}}{4 - \bar{\eta}_{\mathbf{K}_n}}, \tag{1.15}$$

and where

$$\bar{\eta}_{\mathbf{K}_n} = \frac{k_B T}{4\pi} \frac{3\mu + \lambda}{\mu(2\mu + \lambda)} \mathbf{K}_n^2 \tag{1.16}$$

is the exponent with which the real-space density-density correlation function decays in a 2D crystal *without* a substrate potential [5]. We therefore predict that for $T < T_m(0)$ the intensity of the on-q_y-axis Bragg peaks vanishes as an *exact* power of the input laser intensity $I_{\rm in}$, according to

$$I_{\rm out}(\mathbf{K}_n) \sim |\langle \rho_{\mathbf{K}_n} \rangle|^2 I_{\rm in}, \tag{1.17a}$$

$$\sim I_{\rm in}^{1 + 2/\delta_M}. \tag{1.17b}$$

In contrast, we predict the intensity $I_{\rm out}$ of the off-axis quasi-Bragg peaks, labeled by a reciprocal wave vector $\mathbf{G}$, to vanish as

$$I_{\rm out}(\mathbf{G}) \sim I_{\rm in}^{1 + 2\hat{\eta}_{\mathbf{G}}/(4 - \hat{\eta}_{\mathbf{G}})} L^{2 - (\bar{\eta}_{\mathbf{G}} - \hat{\eta}_{\mathbf{G}})}, \tag{1.18}$$

where

$$\hat{\eta}_{\mathbf{G}} \equiv \bar{\eta}_{\mathbf{G}}(1 - G_x^2/G^2), \tag{1.19}$$

and L is the system size.

We can also define the translational correlation length by the widths of the off-q_y-axis Lorentzian peaks in the structure function. As the melting temperature T_m is approached from above, given the XY nature of the $p=1$ LFS melting phase transition, we expect the correlation lengths parallel and perpendicular to the troughs to diverge according to

$$\xi_{x,y} \sim e^{c/|T - T_m|^{1/2}}, \tag{1.20}$$

where c is a constant of order unity.

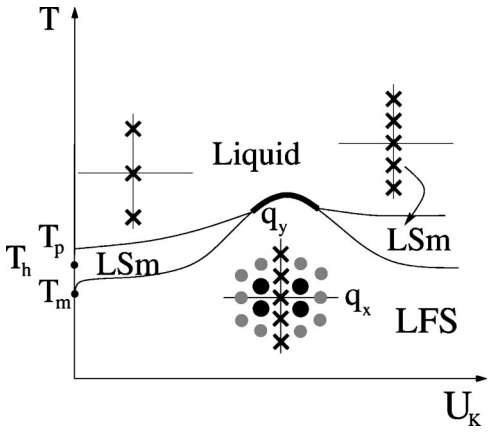

FIG. 4. Schematic phase diagram for a primary commensurate orientation with a commensurability parameter in the range $1<p<p_c$ (the case $p=2$ is shown here). Thin lines indicate continuous phase transitions. The thick line between the LFS and the modulated liquid phase is most likely a first order phase boundary. *Insets:* Schematic structure functions. As in Fig. 2, the $\times$'s indicate delta-function Bragg peaks, and the shaded circles algebraic peaks.

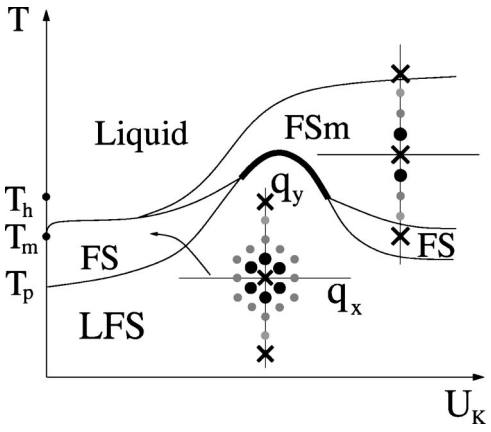

FIG. 5. Schematic phase diagram for a primary commensurate orientation with a commensurability parameter $p>p_c$ (the case $p=4$ is shown here). As in Fig. 4, the thick line indicates a first order transition. *Insets:* Schematic structure factors. As in Fig. 4, the $\times$'s indicate delta-function Bragg peaks, and the shaded circles algebraic peaks.

2. Intermediate commensurability ratios: $1<p<p_c$

For $1<p<p_c$, the phase diagram, illustrated in Fig. 4, generically includes an additional symmetry-allowed ''locked smectic'' (LSm) phase. The LSm phase distinguishes itself from the modulated liquid by spontaneously breaking the liquid's discrete translational symmetry by d down to translations by pd [33]. In contrast to the LFS phase, however, the LSm phase exhibits only short-range correlations between colloidal positions lying in different troughs, and therefore does not resist shear deformations for displacements along the potential minima. Correspondingly, as illustrated in Fig. 4, the structure function of the LSm phase displays spontaneously induced Bragg peaks at $\mathbf{K}_n/p$, in addition to the Bragg peaks at $\mathbf{K}_n$, directly induced by the laser interference fringes. For $1<p<p_c$, the LFS phase also displays these spontaneous Bragg peaks on the q_y axis at $\mathbf{q}=\mathbf{K}_n/p$.

Symmetry dictates that the freezing of the modulated liquid into the LSm phase is in the *p-state clock* model universality class. Also, similar to the melting of the $p=1$ LFS, we find that the $1<p<p_c$ LFS phase melts into a LSm phase through a transition in the XY universality class, and will therefore also exhibit the usual Kosterlitz-Thouless phenomenology [4]. We have also added to the phase diagram the possibility of a direct transition from a LFS phase to a modulated liquid phase at intermediate potential strength. We expect this transition to be different than the LFS-liquid transition for $p=1$. Whereas the $p=1$ transition is in the XY universality class, for $1<p<p_c$ the LFS-liquid transition is associated with simultaneous loss of XY and discrete (Ising for $p=2$) order. Because at this latter transition two unrelated symmetries are simultaneously restored, we expect it to be first order. At the multicritical point, where the liquid, LFS, and LSm phases meet, the critical behavior is presumably described by a two-dimensional compressible Ising model (for $p=2$) [34] of the form

$$H_{\mathrm{I}-XY}[u,S]=\int d^2r\left[\tfrac{1}{2}(\nabla S)^2+\tfrac{1}{2}rS^2+vS^4\right]+H_{\mathrm{LFS}}[u]+\int d^2r(\gamma_x\partial_x u_x+\gamma_y\partial_y u_x)S^2. \tag{1.21}$$

S is a continuous Ising order parameter, that distinguishes the LSm phase from the liquid phase; $\gamma_{x,y}$ are ''magnetoelastic'' parameters, which couple the elastic strain to the ''magnetization'' S, and where the parameters of the model are tuned to the tricritical point at which both order parameters vanish simultaneously. It would be interesting to study the properties of such a tricritical point, which to our knowledge has not been previously explored.

3. Large commensurability ratios and floating phases: $p>p_c$

For these higher values of p, the complexity of the 2D colloidal phase diagram (displayed in Fig. 5) further increases, allowing two new phases, the ''floating solid'' (FS) and the ''floating smectic'' (FSm) phases.

The new phases are distinguished from their ''locked'' counterparts, the LFS and LSm phases, by their ability to slide (float) *across* the troughs of the periodic potential; technically, the periodic potential is irrelevant (in the renormalization group sense), and therefore can be treated perturbatively inside the FS and FSm phases. As illustrated in Fig. 5, all the *spontaneously* induced structure function peaks of these floating phases are *quasi*-Bragg peaks, and therefore the corresponding density correlation functions display real-space *power-law* decays, similar to Eq. (1.12). Although, in principle, the critical values p_c^{S} and p_c^{Sm} for the appearance of each of these floating phases are most likely distinct, for simplicity of the presentation we have taken $p_c^{\mathrm{S}}=p_c^{\mathrm{Sm}}\equiv p_c$. If in reality these critical values are sufficiently distinct, and $p_c^{\mathrm{S}}<p_c^{\mathrm{Sm}}$, then we expect an intermediate range of p values, $p_c^{\mathrm{S}}<p<p_c^{\mathrm{Sm}}$, for which no FSm appears.

We find that phase transitions between the corresponding locked and floating phases (LFS-FS and LSm-FSm) are in the same universality class as the well-known thermal rough-

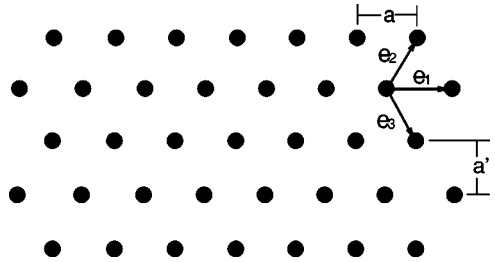

FIG. 6. Perturbation-free ideal hexagonal colloidal crystal, characterized by fundamental lattice vectors $\mathbf{e}_i$.

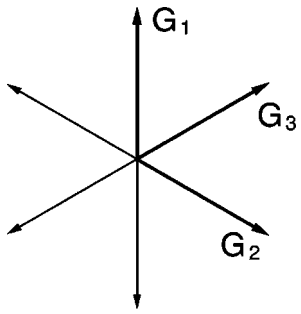

FIG. 7. A set of three fundamental reciprocal lattice vectors $\mathbf{G}_i$, which completely characterize a perfect hexagonal lattice.

ening transition [35], the dual of the Kosterlitz-Thouless (KT) transition, with an identical phenomenology. Similar to the XY-melting LFS-LSm transition discussed above, the melting of the FS phase into the FSm phase proceeds via an unbinding of dislocation pairs with x-directed Burgers vectors. However, because of the presence of massless spectator phonon modes in the y direction (transverse to the troughs of the periodic potential), the melting of the FS phase into the FSm phase might be modified.

The direct transition from LFS to FSm phases is most likely first order. Here the order of the u_x modes changes from quasi-long-range to short-range (via an unbinding of type I dislocations, i.e., those with Burgers vector parallel to the troughs of the periodic potential), and those of the u_y modes from long-range to quasi-long-range (via a depinning from the laser potential, i.e., a roughening transition). If both order parameters become critical at the same point in the phase diagram, which will be the case at multicritical points where the FS, LFS, and FSm phases meet, we have a phase transition corresponds a simultaneous transition of the KT type and its dual analog.

The remainder of this paper is organized as follows: in Sec. II, we introduce and motivate our model for 2D solids subjected to a 1D periodic potential, and discuss the details specific to the experiments on 2D colloids in the laser potential [22]. In Sec. III, we give a detailed analysis of all the phases which are allowed by symmetry. In particular, the static structure factors and correlation functions are discussed. The mechanisms—dislocation, unbinding and soliton proliferation—driving the phase transitions are investigated in Sec. IV. In Sec. V we derive the universal features of the melting phase boundary, demonstrating that for sufficiently short-range interactions it generically exhibits a reentrant melting observed in the experiments of Wei *et al.* [22]. Some aspects of the response of the translational and bond-orientational order parameter to a small external 1D periodic potential are analyzed in Sec. VI using a renormlization group (RG) crossover analysis. In Sec. VII we elaborate on some implications of our results to experiments and for computer simulations.

II. BASIC INGREDIENTS

A. ''Microscopic'' model

In the absence of external perturbations, we expect that, at sufficiently low temperatures the 2D colloidal system freezes into a hexagonal 2D crystal illustrated in Fig. 6. Its lattice sites $\mathbf{r}_n = n_1\mathbf{e}_1 + n_2\mathbf{e}_2$, with $n_{1,2} \in \mathcal{Z}$, are spanned by a set of lattice vectors

$$\mathbf{e}_1 = a\hat{\mathbf{e}}_x, \tag{2.1a}$$

$$\mathbf{e}_2 = \frac{a}{2}(\hat{\mathbf{e}}_x + \sqrt{3}\hat{\mathbf{e}}_y), \tag{2.1b}$$

$$\mathbf{e}_3 = \frac{a}{2}(\hat{\mathbf{e}}_x - \sqrt{3}\hat{\mathbf{e}}_y), \tag{2.1c}$$

or equivalently, in Fourier space, the lattice is characterized by a set of three fundamental reciprocal lattice vectors (see Fig. 7)

$$\mathbf{G}_1 = \frac{2\pi}{a'}\hat{\mathbf{e}}_y, \tag{2.2a}$$

$$\mathbf{G}_2 = \frac{\pi}{a'}(\sqrt{3}\hat{\mathbf{e}}_x - \hat{\mathbf{e}}_y), \tag{2.2b}$$

$$\mathbf{G}_3 = \frac{\pi}{a'}(\sqrt{3}\hat{\mathbf{e}}_x + \hat{\mathbf{e}}_y), \tag{2.2c}$$

with $a' = a\sqrt{3}/2$, and a the mean colloidal spacing related to the particle density ρ by $\rho = 2/(\sqrt{3}a^2)$.

At sufficiently long scales [36] and to quadratic order in the elastic strain,

$$u_{ij} = \tfrac{1}{2}(\partial_i u_j + \partial_j u_i), \tag{2.3}$$

associated with the colloidal displacement field $\mathbf{u}(x,y)$ relative to the equilibrium position in the unconstrained solid, the elastic energy of a 2D hexagonal crystal is well described by the continuum isotropic elastic Hamiltonian

$$H_0 = \frac{1}{2}\int d^2r(2\mu u_{ij}^2 + \lambda u_{kk}^2). \tag{2.4}$$

The Lamé coefficients μ and λ, with μ the usual shear modulus, are the only two elastic constants necessary to completely characterize the elastic energy associated with small deformations of an unperturbed 2D hexagonal solid.

An applied 1D periodic potential, which in experiments [16,22] with dielectric colloidal spheres is conveniently cre-

ated by two interfering laser beams, is easily incorporated as an additional energetic contribution $H_{\mathbf{K}}$,

$$H_{\mathbf{K}} = -U_K \frac{\sqrt{3}}{2} \sum_n \cos\{\mathbf{K}\cdot[\mathbf{r}_n + \mathbf{u}(\mathbf{r}_n)]\}, \tag{2.5}$$

where we have focused on the energetically most important *lowest* harmonic **K** of such a laser-induced potential. The coupling U_K measures the strength of the **K**th harmonic of the laser potential, proportional to the input laser intensity I_{in}.

For the purpose of the discussion in this section we have chosen an ''internal'' reference frame $(\hat{\mathbf{e}}_x, \hat{\mathbf{e}}_y)$ where the orientation of the hexagonal lattice is kept fixed. Later, beginning with Sec. III we will switch to a ''laboratory frame'' $(\hat{\mathbf{x}}, \hat{\mathbf{y}})$ where the orientation of the laser potential is fixed with $\mathbf{K} \| \hat{\mathbf{y}}$, i.e., with the troughs running parallel to the $\hat{\mathbf{x}}$ axis.

B. Commensurability and reciprocal lattice

For a general wave vector **K**, the periodic (laser) potential—characterized by a plane wave, $e^{i\mathbf{K}\cdot\mathbf{r}}$—will not be commensurate with the hexagonal lattice. Only for a particular orientation and magnitude of **K** will the spacing between the potential minima match with the periodicity of the hexagonal lattice. It is this special set of *commensurate* periodic potentials that is the focus of our work here. The characteristic set of commensurate wave vectors is easy to find since the reciprocal lattice is *defined* to be the set of all wave vectors **G** that yield plane waves with the periodicity of a given Bravais lattice. Hence commensurability is equivalent to the condition that **K** coincides with one of the reciprocal lattice vectors **G**.

In other words, the planes defined by the minima of the external potential $[\cos(\mathbf{K}\cdot\mathbf{r})]$ are a superset of the family of lattice planes (Bragg planes) defined by the shortest reciprocal lattice vector $\mathbf{G}_{\vec{m}} = m_1\mathbf{G}_1 + m_2\mathbf{G}_2$, with Miller indices m_1 and m_2, parallel to the wave vector of the external potential **K**:

$$\mathbf{K} = p\mathbf{G}_{\vec{m}} = p_1\mathbf{G}_1 + p_2\mathbf{G}_2. \tag{2.6}$$

Note that here we focus on situations where the colloidal particles are allowed to sit in the minima of the external potential only. More generally, one could also consider situations where the commensurability parameter is less than 1 with p a rational fraction [30].

With $d = 2\pi/|\mathbf{K}|$ being the periodicity of the potential and $a'_{\vec{m}} = 2\pi/|\mathbf{G}_{\vec{m}}|$ defining the distance between the lattice planes, the *commensurability ratio* p is given by

$$p \equiv \frac{a'_{\vec{m}}}{d} = \frac{|\mathbf{K}|}{|\mathbf{G}_{\vec{m}}|} \tag{2.7a}$$

$$= \frac{\sqrt{3}a/2}{d}(m_1^2 + m_2^2 - m_1 m_2)^{-1/2}. \tag{2.7b}$$

This allows us to characterize the laser potential by a set of Miller indices $\vec{m} = (m_1, m_2)$, and the commensurability ratio p, i.e., in summary by a commensurability vector $\vec{p} = p\vec{m} = (p_1, p_2)$. Equivalently, the orientation of the Bragg planes can also be characterized by the shortest direct lattice vector pointing parallel to the troughs of the external potential,

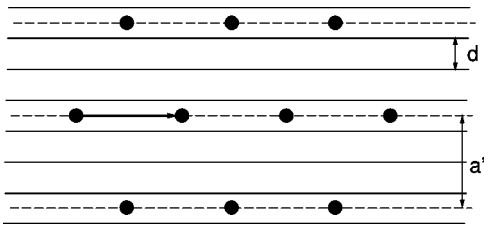

FIG. 8. 2D hexagonal colloidal crystal in the presence of a commensurate 1D periodic potential with period d, commensurability vector $\vec{p} = 3(1,0)$, and potential maxima indicated by solid lines. Dashed lines denote the Bragg rows picked out by the laser potential minima.

$$\mathbf{R}_{\vec{n}} \equiv n_1\mathbf{e}_1 + n_2\mathbf{e}_2, \tag{2.8}$$

with the condition $\mathbf{R}_{\vec{n}} \cdot \mathbf{G}_{\vec{m}} = 0$, i.e., $(n_1, n_2) = (m_1, -m_2)$ a set of integers (direct lattice Miller indices), with no common factor complementary to the Miller indices.

In Fig. 8 we displayed an example for the simplest set of relative orientations between the periodic potential and the colloidal crystal. In our notation this corresponds to an orientation $(m_1, m_2) = (1,0)$ [or, equivalently, $(n_1, n_2) = (1,0)$] and a commensurability ratio $p = 3$, i.e., $\mathbf{K} = 3\mathbf{G}_{(1,0)} = 3\mathbf{G}_1$ and a Bragg row spacing $a'_{\vec{m}} = a' = a\sqrt{3}/2$. Because in such $\vec{m} = (1,0)$ orientations, it is *primary* Bragg rows [28] that run parallel to the periodic potential troughs, we call these relative orientations ''primary.'' Aside from the simplicity of these configurations, our interest in them is driven by experiments in Refs. [16,22], where a primary $p = 1$ orientation was studied.

In addition to these primary $\vec{p} = p(1,0)$ configurations, we will also make detailed predictions for the next simplest $\vec{p} = p(1,-1)$ set of relative lattice-laser potential configurations, illustrated for $p = 1$ in Fig. 9. We call these orientations ''dual primary,'' because they correspond to Bragg rows running perpendicular to a *fundamental real-space* lattice vector with $\mathbf{K} = p(\mathbf{G}_1 - \mathbf{G}_2) = -\mathbf{e}_3 4\pi/a^2$, rather than to one of the three *fundamental reciprocal* lattice vectors. In terms of the direct lattice these dual-primary orientations correspond to $(n_1, n_2) = (1,1)$ and Bragg row spacing $a'_{\vec{m}} = a/2$. An example of a more general orientation is illustrated in Fig. 10.

Using the definition of commensurate configurations [Eq. (2.6)], in Eq. (2.5), we find that $H_{\mathbf{K}}$ reduces to

$$H_{\mathbf{K}} = -U_K \frac{\sqrt{3}}{2} \sum_{\mathbf{r}_n} \cos[\mathbf{K}\cdot\mathbf{u}(\mathbf{r}_n)], \tag{2.9a}$$

$$= -U_K a^{-2} \int d^2 r \cos[\mathbf{K}\cdot\mathbf{u}(\mathbf{r})], \tag{2.9b}$$

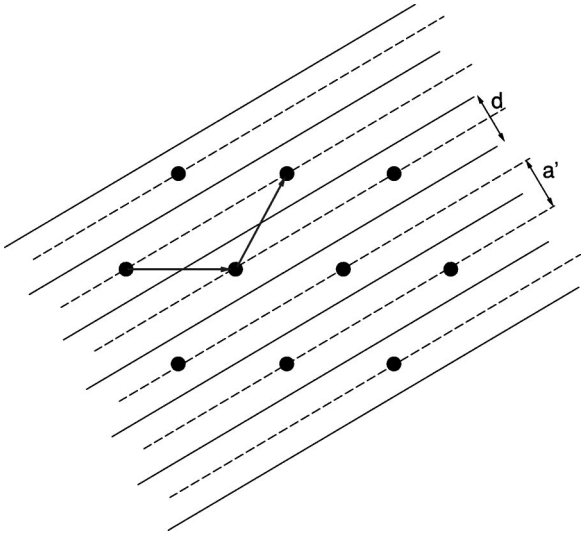

FIG. 9. 2D hexagonal colloidal crystal in the presence of a commensurate 1D periodic potential with period d, commensurability vector $\vec{p}=(1,-1)$, and potential maxima indicated by solid lines. Dashed lines denote the Bragg rows picked out by the laser potential minima.

where in going from Eq. (2.9a) to Eq. (2.9b) we went over to a continuum description, an innocuous approximation for the smooth $|\mathbf{u}(\mathbf{r}_{n+1})-\mathbf{u}(\mathbf{r}_n)|\ll a$ distortions, that we study here.

An equivalent ''soft-spin'' continuum description of the above interaction is in terms of the elementary translational order parameters $\rho_{\mathbf{G}_i}(\mathbf{r})=\rho^0_{\mathbf{G}_i}e^{i\mathbf{G}_i\cdot[\mathbf{r}+\mathbf{u}(\mathbf{r})]}$, with $i=1$ and 2. The laser-induced periodic potential $h_{\mathbf{K}}(\mathbf{r})=\mathrm{Re}[h^0_{\mathbf{K}}e^{i\mathbf{K}\cdot\mathbf{r}}]$ acts like an ordering field on the $\vec{p}=\pm(p_1,p_2)$th harmonics of the fundamental order parameters $\rho_{\mathbf{G}_i}(\mathbf{r})$, allowing a linear coupling to $\rho_{\pm\mathbf{G}}(\mathbf{r})=\rho^0_{\pm\mathbf{G}}e^{\pm i\mathbf{G}\cdot[\mathbf{r}+\mathbf{u}(\mathbf{r})]}$,

$$H_{\mathbf{K}}=-\alpha\int d^2r[h^*_{\mathbf{K}}(\mathbf{r})\rho_{\mathbf{G}}(\mathbf{r})+\mathrm{c.c.}] \tag{2.10a}$$

$$=-\alpha\rho^0_{\mathbf{G}}h^0_{\mathbf{K}}\int d^2r[e^{i(\mathbf{G}-\mathbf{K})\cdot\mathbf{r}}e^{i\mathbf{G}\cdot\mathbf{u}}+\mathrm{c.c.}], \tag{2.10b}$$

which is finite at long scales only if the condition Eq. (2.6) is satisfied, in which case it reduces to the expression given in Eq. (2.9b), with the identification $U_K/a^2=2\alpha\rho^0_{\mathbf{G}}h^0_{\mathbf{K}}$. Hence the periodic potential explicitly breaks translational symmetry and therefore induces a finite translational order parameters $\rho_{\pm\mathbf{K}}(r)$ throughout the phase diagram.

C. Broken rotational symmetry and anisotropic elasticity

Throughout our phase diagram, the imposed 1D periodic potential also *explicitly* breaks down the 2D rotational symmetry to $\mathcal{Z}_2$ (Ising) symmetry, corresponding to rotations by π. We can see this more explicitly by noting that the laser potential $h_{\mathbf{K}}(\mathbf{r})=\mathrm{Re}[h^0_{\mathbf{K}}e^{i\mathbf{K}\cdot\mathbf{r}}]$ generates a set of even-rank tensor fields,

$$h^{(2n)}_{i_1\ldots i_{2n}}=\overline{\partial_{i_1}h_{\mathbf{K}}(\mathbf{r})\partial_{i_2}h_{\mathbf{K}}(\mathbf{r})\ldots\partial_{i_{2n}}h_{\mathbf{K}}(\mathbf{r})}, \tag{2.11}$$

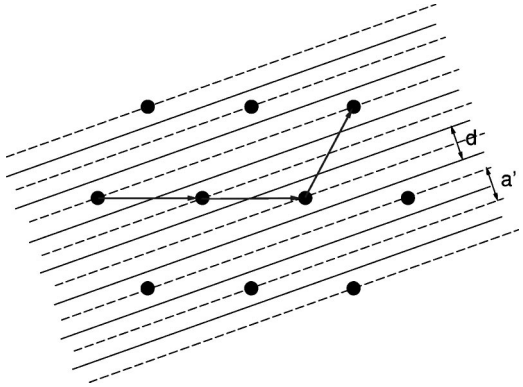

FIG. 10. 2D hexagonal colloidal crystal in the presence of a commensurate 1D periodic potential with period d, commensurability vector $\vec{p}=(2,-1)$, and potential maxima indicated by solid lines. Dashed lines denote the Bragg rows picked out by the laser potential minima.

where in above the overline denotes a spatial average. The lowest order, rank 2, tensor field is given by

$$h^{(2)}_{ij}=\overline{\partial_i h_{\mathbf{K}}(\mathbf{r})\partial_j h_{\mathbf{K}}(\mathbf{r})}, \tag{2.12a}$$

$$=\tfrac{1}{2}|h^0_{\mathbf{K}}|^2K_iK_j. \tag{2.12b}$$

It is clear from their definition that these laser-generated $2n$-rank tensor fields have strengths proportional to $(U_K)^{2n}\propto(I_{\mathrm{in}})^{2n}$. They act as external ordering fields, which explicitly break rotational invariance (modulo rotations by π) of our system and therefore induce throughout our phase diagram finite $2n$-adic orientational order parameters. These can be characterized by rank-$2n$ symmetric traceless tensors, which are real irreducible representations of the rotation group, and are the ''angular harmonics'' of the lowest order (rank 2) nematic order parameter

$$Q^{(2)}_{ij}=S(\hat{n}_i\hat{n}_j-\tfrac{1}{2}\delta_{ij}). \tag{2.13}$$

The unit vector $\hat{\mathbf{n}}$ defines the principal axis of the nematic order, and, given Eq. (2.12b), points parallel or perpendicular (depending on the sign of the coupling between $h^{(2)}_{ij}$ and $Q^{(2)}_{ij}$) to the periodic potential wave vector $\mathbf{K}$. In two dimensions these $2n$-rank tensor representations are well-known to be equivalent to the one-dimensional complex irreducible representations

$$\psi_{2n}=e^{i2n\theta}. \tag{2.14}$$

Since in the presence of these laser-induced ordering fields all ψ_{2n} orientational order parameters are finite throughout our phase diagram, no sharp continuous *orientational* ordering phase transitions are possible in our system. This is in contrast to the melting of the unperturbed lattice, where a thermodynamically sharp orientational phase transition is allowed between the isotropic and the anisotropic (e.g., hexatic, in a hexagonal lattice) liquids [5]. Therefore,

throughout this paper we confine our attention only to phases and phase transitions that *spontaneously* break the *translational* symmetry of the explicitly orientationally ordered, modulated colloidal liquid phase.

The existence of these orientational ordering fields h_{2n} has important consequences to the form of the colloidal crystal elastic energy. To deduce the form of the appropriate elastic Hamiltonian, it is instructive first to consider a 2D hexagonal lattice in the absence of such *explicit* symmetry breaking fields. Such a state is characterized by a finite value of the hexagonal orientational order parameter ψ_6 [5], with the full 2D rotational symmetry broken down to the symmetry of discrete rotations by $2\pi/6$. Nevertheless to a quadratic order in the strain tensor u_{ij}, the energy is invariant under a full 2D rotation group.

In the absence of a periodic potential the hexagonal orientational order can be further *spontaneously* broken down to a lower symmetry. A physically important example is a uniaxially distorted hexagonal 2D crystal of anisotropic, orientationally ordered, molecules, as, for instance found in a nematic liquid crystal. Such a system exhibits a *spontaneous* nematic order parameter $Q_{ij}^{(2)}$, which modifies the isotropic elasticity H_0 [Eq. (2.4)]. To a quadratic order in the strain u_{ij}, three additional energetic contributions

$$\delta H_0 = \int d^2r[\alpha_1 u_{ij} Q_{ij}^{(2)} + \alpha_2 (u_{ij} Q_{ij}^{(2)})^2 + \alpha_3 u_{ij} u_{jk} Q_{ki}^{(2)}] \tag{2.15}$$

are allowed. Because the nematic order is induced spontaneously, simultaneous rotations of the lattice degrees of freedom and of the nematic axis (encoded in $Q_{ij}^{(2)}$), relative to an arbitrary frame fixed in the lab, are clearly symmetries of such a uniaxially distorted lattice. It is not difficult to show that this rotational freedom allows us to eliminate α_1 coupling linear in u_{ij},

$$H_{\alpha_1} = \alpha_1 S \int d^2r[u_{xx}(\sin^2\theta - \tfrac{1}{2}) + u_{yy}(\cos^2\theta - \tfrac{1}{2}) + u_{xy} 2\sin\theta\cos\theta], \tag{2.16}$$

by a judicious choice of the rotation angle θ and a uniaxial area-preserving distortion

$$u_i \rightarrow u_i + \phi_i . \tag{2.17}$$

It is important to note that this is only possible because the three independent degrees of freedom, θ, ϕ_x and ϕ_y, at our disposal are sufficient to cancel the three independent linear terms u_{xx}, u_{yy}, and u_{xy} in H_{α_1} [Eq. (2.16)].

Adding H_{α_2} and H_{α_3} contributions [Eq. (2.15)], to the Hamiltonian of an undistorted hexagonal lattice [Eq. (2.4)], we find a general elastic Hamiltonian for a *spontaneously* uniaxially distorted hexagonal lattice (in the absence of an external potential) [37] given by

$$H_0^a = \int d^2r[2\mu u_{xy}^2 + \tfrac{1}{2}\lambda_{xx} u_{xx}^2 + \tfrac{1}{2}\lambda_{yy} u_{yy}^2 + \lambda_{xy} u_{xx} u_{yy}], \tag{2.18}$$

where we have chosen a coordinate system in which the x and y axes coincide with the $\hat{\mathbf{n}}$ and $\hat{\mathbf{z}}\times\hat{\mathbf{n}}$ principal axes of the orientational nematic order parameter $Q_{ij}^{(2)}$. The two *additional* elastic constants, a total of four in H_0^a, are consistent with two new couplings α_2 and α_3 allowed by the finite orientational nematic order parameter $Q_{ij}^{(2)}$. The four independent elastic constants also coincide with the expectation that, with the symmetry between x and y broken, the elastic energies associated with the strain tensor components

$$u_{xx} = \partial_x u_x , \tag{2.19a}$$

$$u_{yy} = \partial_y u_y , \tag{2.19b}$$

$$u_{xy} = \tfrac{1}{2}(\partial_x u_y + \partial_y u_x) \tag{2.19c}$$

are clearly independent. Although rotations relative to the orientational uniaxial order is no longer a symmetry of H_0^a, because only the *symmetric* strain tensor u_{ij} enters the elastic energy, H_0^a is still invariant under ''atomic'' displacements,

$$\mathbf{u} = \theta\hat{\mathbf{z}}\times\mathbf{r}, \tag{2.20}$$

which correspond to *global* rigid rotations of the 2D solid, by an infinitesimal angle θ about the z axis. This latter symmetry is clearly present in an anisotropic lattice *without* an external pinning potential.

In contrast, however, in our system, the 1D periodic potential has a *fixed* orientation in the laboratory frame. Hence, in addition to the uniaxial lattice anisotropy, such a potential also explicitly breaks the symmetry of rotations relative to the lab (and therefore to the periodic potential) frame. It therefore picks out a special coordinate system relative to which the angle θ is measured.

As discussed above such external potential acts as an external $2n$-rank tensor fields, and explicitly breaks the corresponding orientational symmetry. The appropriate elastic energy can be deduced by focusing on the lowest order nematic ordering field $h_{ij}^{(2)}$. It allows the additional energetic contributions

$$H_{h_2} = -\int d^2r[u_{ij} h_{ij}^{(2)} + Q_{ij}^{(2)} h_{ij}^{(2)}], \tag{2.21}$$

that explicitly break the symmetry of rotations relative to the frame picked out by the periodic potential.

For purposes of classification of the relative orientations discussed in Sec. II B, it was more convenient to keep the lattice fixed and to rotate the periodic potential into a particular orientation, uniquely labeled by an integer 2D Miller index vector $\vec{p} = (p_1, p_2)$. However, once an orientation has been selected and classified by $\vec{p}$, to analyze the continuum elastic model and its thermodynamics that follows it is more convenient to work in a coordinate system in which, instead, the troughs of the 1D periodic potential run along the new x axis. For such a choice of a lab coordinate system,

$$h_{ij}^{(2)} = \tfrac{1}{2}|h_{\mathbf{K}}^0|^2 K^2 \hat{y}_i \hat{y}_j . \tag{2.22}$$

Using this expression for $h_{ij}^{(2)}$ together with that for Q_{ij} [Eq. (2.13) inside of Eq. (2.21)], and combining it with H_{α_1} [Eq. (2.16)], we find the following symmetry breaking energetic contribution, which, in the presence of a 1D periodic potential must be added to H_0^a [Eq. (2.18)]:

$$H_{\alpha_1+h_2}=\int d^2r\Bigg[\alpha_1 S u_{xx}\Big(\sin^2\theta-\frac{1}{2}\Big)+u_{yy}\Big(\alpha_1 S\cos^2\theta-\frac{\alpha_1 S}{2}-h\Big)+\alpha_1 S u_{xy}\sin 2\theta-\frac{1}{2}hS\cos 2\theta\Bigg], \tag{2.23}$$

where $h\equiv\frac{1}{2}K^2|h_{\mathbf{K}}^0|^2$, and angle θ measures the deviation of the nematic axis $\hat{\mathbf{n}}$ away from $\mathbf{K}$ set by the orientation of the periodic potential. While it is still possible to eliminate the terms linear in u_{xx} and u_{yy} by a lattice distortion Eq. (2.17), in the presence of the external potential it is no longer possible to shift away the u_{xy} term. Selecting ϕ_i so as to cancel u_{xx} and u_{yy}, and combining the resulting $H_{\alpha_1+h_2}$ with H_0^a, we find

$$H^a=\int d^2r\Bigg[2\mu u_{xy}^2+\frac{1}{2}\lambda_{xx}u_{xx}^2+\frac{1}{2}\lambda_{yy}u_{yy}^2+\lambda_{xy}u_{xx}u_{yy}+\alpha u_{xy}\sin 2\theta-\frac{\gamma}{2}\cos 2\theta\Bigg], \tag{2.24}$$

where we defined rotational symmetry breaking couplings $\alpha\equiv\alpha_1 S$ and $\gamma\equiv hS$. It is clear from the above α and γ terms in H^a that, in the absence of strain, $u_{xy}=0$, the energy is minimized by $\theta=0$, corresponding to the nematic axis alignment with $\mathbf{K}$, imposed by the periodic potential. In the presence of fluctuations θ will be small but finite. Expanding H^a, above, in these small fluctuations, we obtain a final form of the elastic Hamiltonian characterizing our system

$$H_{\rm el}=\int d^2r\Bigg[2\mu u_{xy}^2+\frac{1}{2}\lambda_{xx}u_{xx}^2+\frac{1}{2}\lambda_{yy}u_{yy}^2+\lambda_{xy}u_{xx}u_{yy}+2\alpha u_{xy}\theta+2\gamma\theta^2\Bigg]. \tag{2.25}$$

Now, to complete our derivation, we must relate the angle θ, characterizing the orientation of the nematic order to the elastic u_i degrees of freedom. We expect that the orientations of the nematic and hexatic order parameters, present in our uniaxially distorted hexagonal lattice, are locked together. Since, in the crystalline phase, fluctuations in this bond orientational order are in turn locked to the local rotation angle induced by the phonon displacements, in the Hamiltonian, Eq. (2.25) we can make the well-known identification

$$\theta=\tfrac{1}{2}(\partial_x u_y-\partial_y u_x), \tag{2.26}$$

thereby completing our derivation. We find that the resulting elastic Hamiltonian, which characterizes a hexagonal lattice in the presence of a 1D periodic potential, involves six elastic constants. While a similar form was suggested, based on symmetry, by Ostlund and Halperin [37] in their analysis of melting of distorted hexagonal crystal films, the α term appearing in our Hamiltonian [Eq. (2.25)] was missed in their expression. As illustrated in Fig. 11, physically, the α term is present because, with troughs running along the x direction, an xy strain will bring particles in Bragg planes lying in the troughs out of alignment with the minima of the periodic potential. This generates a torque which attempts to rotate the lattice and improve the alignment.

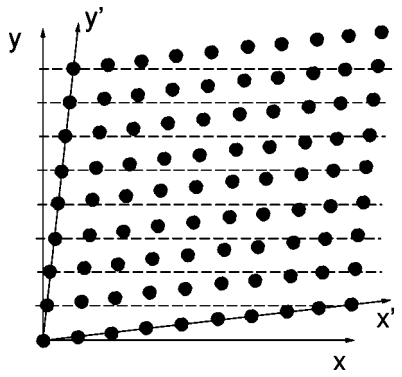

FIG. 11. A $u_{xy}\neq 0$ shear deformation (shown for simplicity for a square lattice) with principal axes along the (1,1) and (1,−1) directions in the xy plane. In the presence of a trough potential (dashed lines) parallel to the x direction, the particle array, with axes x' and y', can lower its interaction energy with the periodic potential by rotating in a clockwise direction to bring the particles into better alignment with the minima in the trough potential.

The elastic Hamiltonian $H_{\rm el}$ [Eq. (2.25)], together with the commensurate pinning potential $H_{\mathbf{K}}$ [Eq. (2.9b)], defines our model 2D colloidal system in the presence of a commensurate periodic laser potential. Our aim in the remainder of the paper is to analyze the symmetry allowed phases and the nature of the transitions between them embodied in this model.

III. SYMMETRY-ALLOWED PHASES

The starting point of our analysis is the model Hamiltonian $H=H_{\rm el}+H_{\mathbf{K}}$, obtained from combining Eqs. (2.9b) and (2.25). Here we have chosen (without loss of generality) $\mathbf{K}$ to lie along the y axis, i.e., the periodic potential troughs running parallel to the x axis, a convention that we will stick to throughout the remainder of the paper. This Hamiltonian admits a rich variety of thermodynamically distinct phases. As discussed in Sec. I, the phase diagrams depend on the commensurability ratio p, or more specifically, in which of the three regimes $p=1$, $1<p\leqslant p_c$, or $p>p_c$, p actually falls. The complexity of the phase diagram is highest for $p>p_c$, and so in order to discuss all the phases possible in our system, we focus on these high p commensurability ratios.

It is convenient to enumerate the five allowed phases starting with the most ordered, which naturally occurs at the lowest temperatures, and proceeding toward the higher temperature disordered phases, by invoking two types of disordering mechanisms: *dislocation unbinding* and *soliton proliferation*. A detailed investigation of these mechanisms is deferred to Sec. IV, where we discuss the nature of these transitions and their hierarchy as a function of temperature

and periodic potential strength (laser intensity). Here we focus on the phases themselves, rather than on their location in the resulting phase diagram. As discussed in detail in Secs. II and I, the imposed periodic potential *explicitly* breaks rotational symmetry, and therefore all five phases exhibit true long-range orientational order. This external potential also explicitly breaks continuous translational symmetry along y (with potential troughs taken to run along x) down to a discrete symmetry of translations by the period d of the potential. Hence all phases will trivially exhibit long-range order in the corresponding translational order parameter, leading to true delta-function Bragg peaks at the multiples of the reciprocal lattice vector $(2\pi/d)\hat{\mathbf{y}}$ in their structure functions.

A. Solid phases

As in the absence of a periodic potential, the most ordered phase of isotropic particles confined to two dimensions is a solid. The striking effect of turning on an external 1D periodic potential is that it can lead to two thermodynamically distinct uniaxially distorted hexagonal crystal phases, which we term a locked floating solid and a floating solid. Being crystalline, both of these phases exhibit 2D translational (quasi-long-range) order, and are characterized by a finite shear modulus. These emerge as a result of breaking the translational symmetry $T_d^y \otimes T^x$ of the ''modulated liquid'' (see below), corresponding to independent discrete translations by $d\hat{\mathbf{y}}$ and continuous translations along $\hat{\mathbf{x}}$, down to 2D discrete translations generated by lattice vectors $\mathbf{e}_1$ and $\mathbf{e}_2$ [Eqs. (2.1a) and (2.1b)]. Although in the presence of thermal fluctuations dislocations will be thermally nucleated, in the solid phases they are confined to finite size dipoles with a zero Burgers ''charge.'' These, therefore, can be safely integrated out of the partition function with only weak *finite* renormalization of the elastic constants. Consequently, a purely elastic description in terms of phonon modes u_x and u_y is appropriate in both phases.

The LFS and FS phases differ in the importance of the periodic pinning potential. In the FS phase, expected to occur at temperatures higher than the LFS phase, thermal fluctuations in the positions of the colloidal particles are sufficiently large such that at long length scales they average away most [38] of the long scale effects of the periodic potential. In contrast, in the LFS phase the periodic potential strongly pins the colloidal crystal transversely to its troughs.

1. Floating solid (FS) phase

A floating solid phase can be rigorously differentiated from its locked counterpart as a 2D colloidal crystal phase in which the periodic potential is *irrelevant* in the renormalization group sense. This implies that at long scales, many, but not all (see below) of the thermodynamic properties of a FS phase are well described by the elastic Hamiltonian $H_{\rm el}$ [Eq. (2.25)], with two coupled ''*massless*'' u_x and u_y degrees of freedom, and ignoring $H_{\mathbf{K}}$. Therefore, in many ways a FS phase is qualitatively quite similar to a 2D solid without the periodic pinning potential. In particular, this similarity extends to the lattice displacement correlation functions which are logarithmic in x and y. However, these similarities do not extend to all correlation functions, and the periodic pinning potential has important qualitative consequences for the FS phase that distinguish it from an ordinary 2D solid. The ''irrelevance'' of the periodic potential means only that a perturbative expansion in U_K, for a sufficiently small value is *convergent*. Consequently, average quantities, that are finite at $U_K=0$, can be well approximated by their $U_K=0$ values, i.e., working with $H\approx H_{\rm el}$, as is usually done. However, quantities that *vanish* (or diverge) to this zeroth order must be evaluated to the next lowest order in U_K to obtain a nontrivial (finite) result.

To illustrate this point, recall that the periodic potential *explicitly* breaks rotational and translational symmetry, despite its irrelevance in the FS phase. While the former leads to uniaxial anisotropy in the hexagonal lattice, the latter is responsible for the true long-range order in the translational order parameter $\rho_{\mathbf{G}}(\mathbf{r})$, with $\mathbf{G}$ integer multiples of the wave vector $\mathbf{K}$ characterizing the periodicity of the external potential. In the presence of the periodic potential, even the most disordered modulated liquid phase (see below) displays true long-range translational and orientational order. Clearly then, a more ordered FS will also break these symmetries.

As a concrete example of how the periodic potential affects the FS phase, consider the real-space two-point correlation function of the translational order parameter

$$\rho_{\mathbf{G}}(\mathbf{r}) \equiv e^{i\mathbf{G}\cdot\mathbf{u}(\mathbf{r})} \tag{3.1}$$

defined by

$$C_{\mathbf{G}}(\mathbf{r}) \equiv \langle \rho_{\mathbf{G}}(\mathbf{r})\rho_{\mathbf{G}}^*(0)\rangle, \tag{3.2a}$$

$$= \langle e^{i\mathbf{G}\cdot[\mathbf{u}(\mathbf{r})-\mathbf{u}(0)]}\rangle, \tag{3.2b}$$

$$\equiv C_{\mathbf{G}}^{(c)}(\mathbf{r}) + \langle \rho_{\mathbf{G}}\rangle\langle \rho_{\mathbf{G}}^*\rangle, \tag{3.2c}$$

where, in Eq. (3.2c), $C_{\mathbf{G}}^{(c)}(\mathbf{r})$ is the connected part of $C_{\mathbf{G}}(\mathbf{r})$. The distinguishing feature of the FS phase is the irrelevance of the periodic potential $H_{\mathbf{K}}$. Hence in the limit of a weak laser potential, i.e., small U_K, we can compute $C_{\mathbf{G}}(\mathbf{r})$ in a controlled, convergent perturbative expansion in U_K. The connected part $C_{\mathbf{G}}^{(c)}(\mathbf{r})$ is nontrivial even to zeroth order in U_K, and a standard calculation gives [5]

$$C_{\mathbf{G}}^{(c)}(\mathbf{r}) \sim \frac{1}{|\mathbf{r}|^{\overline{\eta}_{\mathbf{G}}}}, \tag{3.3}$$

where

$$\overline{\eta}_{\mathbf{G}} = \frac{|\mathbf{G}|^2}{4\pi}\frac{k_B T}{\mu}\frac{3\mu+\lambda}{2\mu+\lambda}. \tag{3.4}$$

For simplicity, we have used the isotropic elastic Hamiltonian [Eq. (2.4)], in place of the correct six elastic constant anisotropic Hamiltonian $H_{\rm el}$ [Eq. (2.25)], which leads to a qualitatively similar, but anisotropic, power-law decay of spatial correlations. We use long wavelength elastic con-

stants finitely renormalized by thermally excited bound dislocation dipoles. We can compute the persistent part of $C_{\mathbf{G}}(\mathbf{r})$, by calculating

$$\langle \rho_{\mathbf{G}} \rangle = \langle e^{i\mathbf{G}\cdot\mathbf{u}(\mathbf{0})} \rangle, \tag{3.5}$$

in a perturbation theory in U_K, which, because of the irrelevance of the periodic potential is convergent in the FS phase. For $U_K = 0$ the translational order parameter vanishes like $\langle \rho_{\mathbf{G}} \rangle_0 = (L/a)^{-\overline{\eta}_{\mathbf{G}}/2}$ with system size $L \to \infty$. Upon expanding the Boltzmann weight $e^{-(H_0+H_{\mathbf{K}})/k_BT}$ in a power series in U_K, we find to leading order in U_K and for $L \to \infty$

$$\langle \rho_{\mathbf{G}} \rangle = \sum_{n=1}^{\infty} \frac{1}{n!} \left(\frac{U_K}{2a^2 k_B T} \right)^n (\delta_{\mathbf{G},n\mathbf{K}} + \delta_{\mathbf{G},-n\mathbf{K}}) \times \prod_{j=1}^{n} \int d^2 r_j \prod_{j=1}^{n} (|\mathbf{r}_j|/a)^{-n\overline{\eta}_{\mathbf{K}}} \prod_{i<j}^{n} (|\mathbf{r}_i - \mathbf{r}_j|/a)^{-\overline{\eta}_{\mathbf{K}}}. \tag{3.6}$$

Here we have used the fact that for $L \to \infty$,

$$\left\langle \exp\left[i \sum_{\alpha} \mathbf{q}_\alpha \cdot \mathbf{u}(\mathbf{r}_\alpha) \right] \right\rangle_0 = \exp\left[\sum_{\alpha<\beta} \mathbf{q}_\alpha \cdot \mathbf{q}_\beta G^{(c)}(\mathbf{r}_\alpha - \mathbf{r}_\beta) \right] \tag{3.7}$$

for $\Sigma_\alpha \mathbf{q}_\alpha = \mathbf{0}$, and zero otherwise. We have also introduced a phonon connected correlation function $G^{(c)}(\mathbf{r})$:

$$G^{(c)}(\mathbf{r}) \equiv \tfrac{1}{4} \langle |\mathbf{u}(0) - \mathbf{u}(\mathbf{r})|^2 \rangle_0 . \tag{3.8}$$

Averages with elastic Hamiltonian are designated by $\langle \cdots \rangle_0$. Again approximating $H_{\rm el}$ by its isotropic form H_0 [Eq. (2.4)], a straightforward calculation in the limit $L/a \gg 1$, $r/a \gg 1$ gives

$$G^{(c)}(\mathbf{r}) \approx \frac{\overline{\eta}_{\mathbf{G}}}{G^2} \log(r/a). \tag{3.9}$$

Since U_K is irrelevant in the floating solid phase, the integrals in Eq. (3.6) are IR convergent (i.e., for $L \to \infty$). The power laws appearing in the integrand are implicitly understood to be cut off below the lattice constant a scale by the obvious behavior [see Eq. (3.8)] of the phonon correlation function $\lim_{r\to a} G^{(c)}(\mathbf{r}) = 0$. Upon performing the spatial integrals, which are dominated by the behavior of the connected phonon correlation function at small distances (UV, lattice cutoff a), we obtain, up to nonuniversal factors of order 1,

$$\langle \rho_{\mathbf{G}} \rangle \approx \sum_{n=1}^{\infty} \frac{1}{n!} \left(\frac{U_K}{2a^2 k_B T} \right)^n (\delta_{\mathbf{G},n\mathbf{K}} + \delta_{\mathbf{G},-n\mathbf{K}}). \tag{3.10}$$

Hence, as argued above on physical grounds, despite the irrelevance of the periodic potential, the FS displays true long-range order in the translational order parameter $\rho_{\mathbf{G}}$, with $\mathbf{G}$ satisfying $\mathbf{G} = \pm n\mathbf{K}$, with $C_{\mathbf{G}}(\mathbf{r})$ approaching its asymptotic value as a power law in r. Other translational order parameters, with $\mathbf{G}$ *not* satisfying the above condition, have pure power-law correlation functions, decaying to zero at long separations. In particular, these include the fundamental translational order parameters $\rho_{\mathbf{G}_i}$, which display quasi-long-range order in the FS phase.

Having calculated the translational correlation function $C_{\mathbf{G}}(\mathbf{r})$, the structure function

$$S(\mathbf{q}) = \sum_{\mathbf{r}_m} e^{-i\mathbf{q}\cdot\mathbf{r}_m} C_{\mathbf{q}}(\mathbf{r}_m) \tag{3.11}$$

can now be easily obtained. Using Eqs. (3.2a), (3.3), and (3.10), and taking advantage of the Poisson summation formula to perform the sum over the lattice sites $\mathbf{r}_m$, we find

$$S(\mathbf{q}) \approx \sum_{\mathbf{G}} \frac{1}{|\mathbf{q}-\mathbf{G}|^{2-\overline{\eta}_{\mathbf{G}}}} + \sum_{n=-\infty}^{\infty}{}' A_n \delta^{(2)}(\mathbf{q} - n\mathbf{K}), \tag{3.12}$$

with

$$A_n = \frac{1}{(n!)^2} \left(\frac{U_K}{2a^2 k_B T} \right)^{2n}, \tag{3.13}$$

the prime on the summation in Eq. (3.12) indicating that the $n = 0$ term is excluded.

Equation (3.12) predicts true Bragg peaks (with power-law corrections) at multiples of the periodic potential wave vector $\mathbf{K}$ and pure power-law (quasi-) Bragg peaks at *all other* reciprocal lattice vectors $\mathbf{G}$, even for those with $\mathbf{G} \| \mathbf{K}$. Note that in a real physical system, the periodic potential will *not* in general be a single harmonic, as assumed in our model [Eq. (2.5)]. Hence we expect that the Bragg peak amplitude A_n observed in experiments will be a *sum* of terms like those in Eq. (3.13), and the square of the amplitude of the nth Fourier harmonic $U_{n\mathbf{K}}$ of the applied periodic potential. This of course will only modify the prefactors in the different contributions to $S(\mathbf{q})$, predicted for the FS in Eq. (3.12). We schematically illustrate $S(\mathbf{q})$ for a floating solid in Fig. 12 for the commensurability vectors $\vec{p} = (5,0)$ and $\vec{p} = (2,-2)$, respectively, with the y axis chosen to point along $\mathbf{K}$.

The set of on-$\hat{\mathbf{q}}_y$-axis quasi-Bragg peaks (indicated by open circles) interleaving the true Bragg peaks (indicated by ''x'' 's) is the notable feature that distinguishes the FS from its locked counterpart LFS, in which *all* on-$\hat{\mathbf{q}}_y$-axis peaks are true Bragg peaks.

2. Locked floating solid (LFS) phase

At sufficiently low temperatures, the periodic potential will always be a relevant perturbation, pinning the 2D solid in the direction perpendicular to its troughs. Because of the 1D nature of the pinning potential, a 2D crystal will remain unpinned along the direction of the potential minima, and will be able to adjust freely in that direction. To reflect this dual character, we therefore call this phase the *locked floating solid* phase.

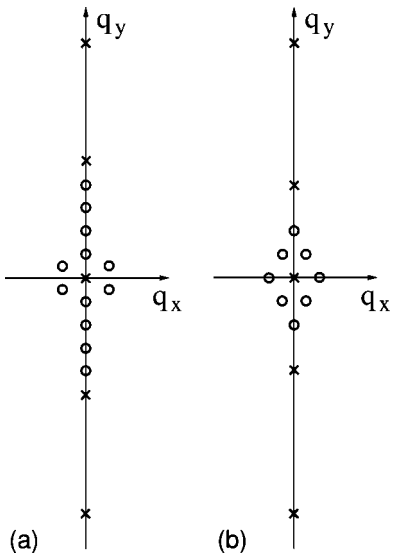

FIG. 12. Schematic structure function for the FS phase with the commensurability vectors (a) $\vec{p}=(5,0)$ and (b) $\vec{p}=(2,-2)$, illustrating a combination of the quasi-Bragg peaks and true Bragg peak, given by Eq. (3.12). Crosses indicate true Bragg peaks, and open circles quasi-Bragg peaks.

At a high laser intensity, such that the bare value of the pinning energy U_K is much larger than the elastic energy μa^2 for the shortest wavelength phonon mode (and therefore all wavelength phonon modes) our system is in the *strong pinning regime*. For a commensurate periodic potential, in this regime, fluctuations in the lattice positions perpendicular to the troughs are small, and the periodic potential $H_{\mathbf{K}}$ [Eq. (2.9)], can be safely expanded in powers of the corresponding phonon degree of freedom, $\mathbf{K}\cdot\mathbf{u}$, leading to

$$H_{\mathbf{K}} \approx \text{const} + \tfrac{1}{2} U_K a^{-2} \int d^2r [\mathbf{K}\cdot\mathbf{u}(\mathbf{r})]^2 \tag{3.14a}$$

$$\approx \text{const} + \tfrac{1}{2} U_K a^{-2} K^2 \int d^2r\, u_y^2(\mathbf{r}). \tag{3.14b}$$

In contrast, a *weak pinning regime* $U_K \ll \mu a^2$ consists of two sets of elastic modes, those with $k<k_c$ and those with $k>k_c$, where $k_c \equiv K/b_*$ is a crossover wave vector for which the elastic energy density $\mu(k_c a)^2$ just balances the pinning energy density $U_K(b_*)K^2$ at the same length scale. Since the pinning energy is subdominate to the elastic energy for modes with $k>k_c$, we can simply integrate out these weakly pinned modes perturbatively in U_K. This results in an effective strength of the pinning potential given by

$$U_K(b_*) = U_K b_*^{-\overline{\eta}_{\mathbf{K}}/2}. \tag{3.15}$$

After equating this with the corresponding elastic energy $\mu(a/b_*)^2$, we find

$$b_* = \left(\frac{\mu a^2}{U_K}\right)^{2/(4-\overline{\eta}_{\mathbf{K}})}, \tag{3.16}$$

which, when inserted inside Eq. (3.15), leads to

$$U_K(b_*) = U_K \left(\frac{U_K}{\mu a^2}\right)^{\overline{\eta}_{\mathbf{K}}/(4-\overline{\eta}_{\mathbf{K}})} \tag{3.17a}$$

$$= U_K^{4/(4-\overline{\eta}_{\mathbf{K}})} / (\mu a^2)^{\overline{\eta}_{\mathbf{K}}/(4-\overline{\eta}_{\mathbf{K}})}. \tag{3.17b}$$

Since the u_y fluctuations in the remaining strongly pinned elastic modes are small, the effective pinning potential $H_{\mathbf{K}}$ can once again be safely expanded in powers of u_y. Doing this we obtain a result identical to Eq. (3.14b), but with U_K replaced by $U_K(b_*)$ given in Eq. (3.17).

Hence, in both strongly and weakly pinned regimes, unlike the FS phase, the LFS phase is characterized at long wavelengths by one acoustic (u_x) phonon mode and one optical (u_y) phonon mode, with an effective Hamiltonian

$$H = H_{\text{el}} + \frac{\mu}{2\xi^2} \int d^2r\, u_y^2(\mathbf{r}). \tag{3.18}$$

Here we have introduced a correlation length ξ which, given Eqs. (3.14b) and (3.17), reads

$$\xi^{-2}(U_K) = \begin{cases} \dfrac{U_K}{\mu a^2} K^2 & \text{for } \dfrac{U_K}{\mu a^2} \gg 1, \\ \left(\dfrac{U_K}{\mu a^2}\right)^{4/(4-\overline{\eta}_{\mathbf{K}})} K^2 & \text{for } \dfrac{U_K}{\mu a^2} \ll 1. \end{cases} \tag{3.19}$$

At length scales longer than the crossover scale set by ξ [Eq. (3.19)], we can safely ignore the spatial derivative of u_y terms, and the LFS phase is well described by an effective Hamiltonian

$$H_{\text{LFS}} = \frac{1}{2} \int d^2r \left[B_{yx} (\partial_y u_x)^2 + B_{xx} (\partial_x u_x)^2 + \frac{\mu}{\xi^2} u_y^2 \right], \tag{3.20}$$

where

$$B_{yx} = (\mu + \gamma - \alpha), \tag{3.21}$$

$$B_{xx} = \lambda_{xx}. \tag{3.22}$$

We can now compute the translational order parameter correlation function and the structure function that characterize the LFS phase. Repeating first the calculation for the persistent part determined by $\langle \rho_{\mathbf{G}} \rangle$, we immediately find, that, as in all the phases in the presence of the periodic potential, $\langle \rho_{\mathbf{G}} \rangle \neq 0$ for $\mathbf{G} = \pm n\mathbf{K}$. However, the distinguishing feature of the LFS is that this average is finite for *all* $\mathbf{G}$ *parallel* to $\mathbf{K}$, by virtue of the finite pinning length ξ [Eq. (3.19)]. This result can be immediately seen by noting that for $\mathbf{G} \| \mathbf{K}$, the logarithmically divergent (with L) $\langle u_x^2 \rangle_0$ correlation function does *not* appear in $\langle \rho_{\mathbf{G}} \rangle_0$, where the subscript 0 again represents an average with the elastic Hamiltonian H_{el} only. Instead we have

$$\langle \rho_{\mathbf{G}} \rangle = e^{-G^2 \langle u_y^2 \rangle / 2} \tag{3.23a}$$

$$= \left(\frac{a}{\xi} \right)^{\overline{\eta}_{\mathbf{G}}/2} \tag{3.23b}$$

which only involves the ''massive'' u_y degree of freedom, whose logarithmic correlations are cut off at $L_c = \xi$, and which is therefore finite even in the thermodynamic limit.

We can also obtain the above result via a straightforward matching calculation. The difficulty of computing translational correlation functions in the weakly pinned regime of the LFS phase is that for long length scales ($>\xi$), despite the weakness of the pinning potential, a direct perturbative expansion in U_K is divergent because of its relevance (in the renormalization group sense) inside the LFS phase. The power of the renormalization group is that it allows us to relate this difficult weakly pinned, small U_K regime to the strongly pinned regime, where U_K has grown to the magnitude of the elastic energy μa^2, and can therefore be treated as a ''mass,'' as in Eq. (3.14b). We can apply this matching procedure to the computation of $\langle \rho_{\mathbf{G}}(U_K) \rangle$ by using a relation between the weakly and strongly pinned regimes, namely,

$$\langle \rho_{\mathbf{G}}(U_K) \rangle = b^{-\overline{\eta}_{\mathbf{G}}/2} \langle \rho_{\mathbf{G}}(U_K b^{2-\overline{\eta}_{\mathbf{K}}/2}) \rangle, \tag{3.24}$$

obtained using the scaling dimension of the operator $\rho_{\mathbf{G}}$ and the RG eigenvalue of U_K, both easily extracted from Eq. (3.3). Choosing the arbitrary rescaling factor $b = b_*$ such that $U_K(b)$ is in the strongly pinned regime, where $U_K(b_*) = \mu a^2$, Eq. (3.24) becomes

$$\langle \rho_{\mathbf{G}}(U_K) \rangle = \left(\frac{U_K}{\mu a^2} \right)^{\overline{\eta}_{\mathbf{G}}/(4-\overline{\eta}_{\mathbf{K}})} \langle \rho_{\mathbf{G}}(\mu a^2) \rangle. \tag{3.25}$$

Since the right hand side is in the strong coupling regime, it can be easily computed using the coarse-grained Hamiltonian [Eq. (3.18)]. Doing this we find

$$\langle \rho_{\mathbf{G}}(U_K) \rangle = \left(\frac{U_K}{\mu a^2} \right)^{\overline{\eta}_{\mathbf{G}}/(4-\overline{\eta}_{\mathbf{K}})} e^{(1/2)\overline{\eta}_{\mathbf{G}} \ln(Ka)}, \tag{3.26}$$

which in the weakly pinned regime is equivalent to the result given in Eq. (3.23b).

Note that the nontrivial nonlinear power-law response of the translational order parameter to the periodic laser potential, predicted by Eq. (3.26) is only a nonanalytic piece of the full response, which includes an analytical background. Hence, although at low temperatures, such that $\overline{\eta}_{\mathbf{G}}/(4-\overline{\eta}_{\mathbf{K}}) < 1$, the full response in the $U_K \to 0$ limit is dominated by the nonanalytical part [Eq. (3.26)], at higher temperatures, the ever-present linear piece of the analytical part will dominate, and experimentally one should instead observe

$$\langle \rho_{\mathbf{G}}(U_K) \rangle \sim U_K. \tag{3.27}$$

For our highly anisotropic system, the connected part of the correlation function $C_{\mathbf{G}}(\mathbf{r})$, is given by

$$C_{\mathbf{G}}^{(c)}(\mathbf{r}) = e^{-(1/2)[G_x^2 G_{xx}(\mathbf{r}) + 2G_x G_y G_{xy}(\mathbf{r}) + G_y^2 G_{yy}(\mathbf{r})]}, \tag{3.28}$$

where $G_{ij}(\mathbf{r}) \equiv \langle [u_i(\mathbf{r}) - u_i(0)][u_j(\mathbf{r}) - u_j(0)] \rangle$ is the connected phonon correlation function computed with the full Hamiltonian. In the weakly pinned regime, for small length scales, all phonon correlation functions display the usual 2D logarithmic growth, which, in the isotropic approximation, i.e., using Hamiltonian H_0 [Eq. (2.4)] leads to the power-law correlation for $C_{\mathbf{G}}^{(c)}(\mathbf{r})$ that we found in Eq. (3.3) for the FS phase. However, for length scales longer than ξ [Eq. (3.19)], while $G_{xx}(\mathbf{r})$ will continue to grow logarithmically, such growth in $G_{yx}(\mathbf{r})$ and $G_{yy}(\mathbf{r})$ will be cut off by the pinning length ξ. Consequently, in the LFS phase we find

$$C_{\mathbf{G}}^{(c)}(\mathbf{r}) \approx \left(\frac{a}{r} \right)^{\eta_{G_x}} \left(\frac{a}{\xi} \right)^{\overline{\eta}_{G_y}}, \tag{3.29}$$

where

$$\eta_{G_x} = \frac{G_x^2}{2\pi} \frac{k_B T}{\sqrt{B_{xx} B_{yx}}} \tag{3.30}$$

which reduces to $\eta_{G_x} = (G_x^2/2\pi)[k_B T/\sqrt{\mu(2\mu+\lambda)}]$ when the effect of the periodic potential on elasticity and renormalizations due to dislocation pairs on the effective elastic coefficients are neglected. A discrete Fourier transform of this correlation function gives the corresponding structure function

$$S(\mathbf{q}) \approx \sum_{\mathbf{G}} \left[\frac{B_G}{|\mathbf{q}-\mathbf{G}|^{2-\eta_{G_x}}} + A_G \delta^{(2)}(\mathbf{q}-\mathbf{G}) \right], \tag{3.31}$$

where the quasi-Bragg peak amplitude B_G is given by

$$B_G \propto \left(\frac{a}{\xi} \right)^{\overline{\eta}_{G_y}} \tag{3.32a}$$

$$\propto \begin{cases} U_K^{\overline{\eta}_{G_y}/2} & \text{for } \dfrac{U_K}{\mu a^2} \gg 1 \\ U_K^{2\overline{\eta}_{G_y}/(4-\overline{\eta}_{\mathbf{K}})} & \text{for } \dfrac{U_K}{\mu a^2} \ll 1 \end{cases} \tag{3.32b}$$

and the Bragg peak amplitude A_G,

$$A_G \propto \delta_{G_x,0} \left(\frac{a}{\xi} \right)^{\overline{\eta}_{\mathbf{G}}} \tag{3.33a}$$

$$\propto \delta_{G_x,0} \begin{cases} U_K^{\overline{\eta}_{\mathbf{G}}/2} & \text{for } \dfrac{U_K}{\mu a^2} \gg 1 \\ U_K^{2\overline{\eta}_{\mathbf{G}}/(4-\overline{\eta}_{\mathbf{K}})} & \text{for } \dfrac{U_K}{\mu a^2} \ll 1, \end{cases} \tag{3.33b}$$

which is finite *if and only if* **G** is parallel to **K**. As a consequence of the discussion after Eq. (3.26), the amplitude A_G

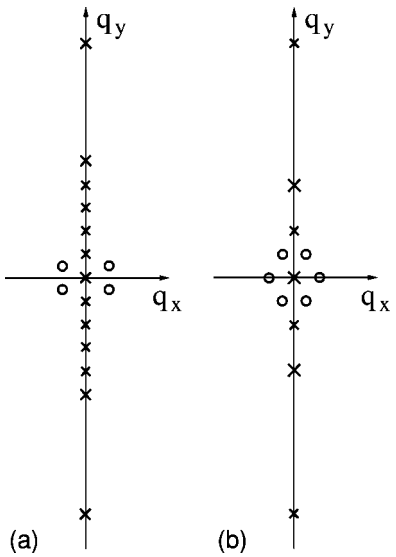

FIG. 13. Schematic structure function for the LFS phase with the commensurability vectors (a) $\vec{p}=(5,0)$ and (b) $\vec{p}=(2,-2)$, illustrating a combination of the quasi-Bragg peaks and true Bragg peaks, given by Eq. (3.31).

will also have a background analytic in U_K, which in a weak pinning limit scales as U_K^2 [see Eq. (3.27)], and therefore at higher temperatures will dominate over the nonanalytical part predicted in Eq. (3.33b).

We illustrate schematically $S(\mathbf{q})$ in Fig. 13 for the commensurability vectors $\vec{p}=(5,0)$ and $\vec{p}=(2,-2)$, respectively, with the y axis chosen to point along **K**.

These predictions for the structure function of the LFS phase, displaying amplitudes that vanish as nontrivial powers (determined by a continuously varying exponent $\overline{\eta}_{G_y}$) of the periodic potential strength [Eqs. (3.32b) and (3.33b)] provide a theoretical explanation for observations of Chowdhury *et al.* [16].

B. Smectic phases

As first pointed out by Ostlund and Halperin [37], in uniaxial two-dimensional lattices, dislocations with Burgers vector along and perpendicular to the uniaxial axis will generically have different core energies, and will therefore proliferate at different temperatures. This will consequently allow the possibility of a phase that is intermediate between a fully ordered crystal and a completely disordered liquid.

In a commensurate orientation, such that Bragg rows coincide with the periodic potential troughs, we would expect dislocation pairs, with Burgers vectors parallel to the potential minima, to unbind first. We refer to the resulting class of thermodynamically distinct phases as smectics. Their main common characteristic is that they display a finite elastic modulus for shear deformations perpendicular to the Burgers vector of unbound dislocations, but do not resist shear parallel to them, possessing only liquidlike correlations between the corresponding ''atomic'' rows. Consequently, such 2D smectics display a 1D periodicity perpendicular to the Burgers vector of unbound dislocations, and, as illustrated in Fig. 14, can be equivalently described as a periodic stack of 1D liquids.

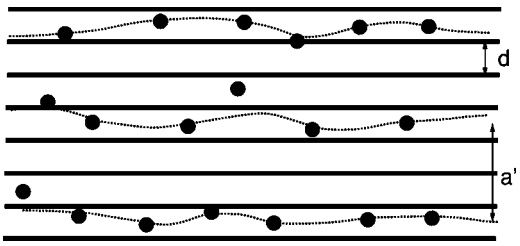

FIG. 14. 2D colloidal smectic phase in the presence of a commensurate 1D periodic potential with period d, commensurability parameter $p=3$, and potential maxima indicated by full horizontal lines. Dashed lines denote the maxima in the smectic density, which are pinned inside the minima of the periodic laser potential.

It is important to note that, despite their name, the smectics discussed here are fundamentally distinct from the smectic phases found in liquid crystal materials and substrate-free smectics discussed in Ref. [37]. The most important distinction is that in liquid crystal smectics and those without an underlying pinning substrate, the orientational symmetry is broken *spontaneously* (uniaxial anisotropy notwithstanding; see Sec. II C), leading to a soft Laplacian-curvature (rather than gradient-tension) elasticity, which preserves this underlying symmetry even in the smectic phase, where it is nonlinearly realized [39,40]. In fact, such substrate-free 2D smectics, because of the softness of their elasticity, are well known to be unstable to thermally driven unbinding of dislocations, and at scales longer than the distance between these free dislocations are therefore indistinguishable from a nematically ordered 2D liquid [41]. As recognized by the authors of Ref. [37], such a thermal instability of substrate-free 2D lattices precludes the existence of a thermodynamically distinct intermediate 2D smectic phase in which only one set of Burgers vectors (e.g., along the uniaxial direction) unbind. However, in strong contrast to those rotationally invariant systems, in the 2D lattices studied here the periodic (laser) potential *explicitly* breaks rotational symmetry, binding by a linear potential dislocation pairs with Burgers vector having components *along* **K**. Consequently, such dislocations remain bound even when those with Burgers vectors *perpendicular* to **K** unbind, and therefore allow the existence of 2D smectic phases that are thermodynamically distinct from a liquid.

Deep in such a smectic phase, the $u_y(\mathbf{r})$ phonon field, which (see Fig. 14) describes local fluctuations in the maxima positions of the 1D density wave, is the only remaining important degree of freedom. The ever-present *bound* dislocation pairs and the density of vacancies and interstitials are ''massive'' degrees of freedom. They can be easily integrated out, leading only to a finite renormalization of elastic constants for u_y deformations, and therefore are unimportant in a static theory.

In close analogy to the translational order parameter of the 2D crystal, a smectic phase is distinguished from a liquid phase by a finite translational order parameter $\rho_{\mathbf{G}}=e^{i\mathbf{G}\cdot\mathbf{u}}$, but with a *single* (rather than a set [Eq. (2.2)]) reciprocal vector

$\mathbf{G}=G\hat{\mathbf{y}}=(2\pi/a)\hat{\mathbf{y}}$. It is related to the total molecular density via a standard relation [39]

$$\rho(\mathbf{r})=\mathrm{Re}[\rho_0+e^{iGy}\rho_{\mathbf{G}}(\mathbf{r})], \tag{3.34}$$

where ρ_0 is the mean density of the smectic.

Of course, in the presence of a 1D periodic potential, a smectic phase is a thermodynamically distinct phase only if $\mathbf{G}=(2\pi/a)\hat{\mathbf{y}}$ differs from the wave vector $\mathbf{K}$ characterizing the external potential and the modulated liquid. Commensurate smectic phases, which we focus on here, are equivalently characterized by the ratio of their period a to that of the periodic potential d, with commensurability ratio $a/d \equiv p \in \mathcal{Z}$. A p-smectic phase then spontaneously breaks the discrete translational symmetry $T_d^y \otimes T^x$ of the modulated liquid, with its equal occupancy of each potential minima down to $T_a^y \otimes T^x$, with only every pth minima equivalently populated. Clearly then $p=1$ smectic is indistinguishable from a fully disordered modulated liquid phase.

Above symmetry considerations uniquely specify the Hamiltonian that characterizes the p-smectic phase,

$$H_{\mathrm{Sm}}=\int d^2r\{\tfrac{1}{2}[B_{xy}(\partial_x u_y)^2+B_{yy}(\partial_y u_y)^2] - U_K a^{-2}\cos[Ku_y(\mathbf{r})]\}, \tag{3.35}$$

which, not surprisingly, is an anisotropic scalar sine-Gordon model in the phonon field $u_y(\mathbf{r})$.

Given the form of the Hamiltonian in Eq. (3.35), there is a close similarity between the properties of the smectic and the 2D crystal studied in Sec. II. The quantitative differences between these phases are due to the distinction between the vector $[\mathbf{u}=(u_x,u_y)]$ and scalar (u_y) natures of elastic degrees of freedom in the 2D solid and smectic phases, respectively. More specifically, in close analogy to the 2D solid phase, we find that for a fixed integer commensurability ratio p, there exist a low temperature ''locked'' and higher temperature ''floating smectic'' phase. These are distinguished by the importance of the periodic pinning potential, which is relevant (in the RG sense) in the LSm phase, acting as a ''mass'' for u_y, and irrelevant in the FSm phase, where for most static properties it can be ignored.

1. Floating smectic (FSm) phase

In the ''floating smectic (FSm) phase,'' thermal fluctuations in the position of the layers are sufficiently large that at long length scales they average away many effects of the periodic pinning potential. Hence, many of the static properties of the FSm phase can be well described by the Hamiltonian [Eq. (3.35)], with $U_K=0$. However, as we discussed in detail in our analysis of the FS phase, despite the RG irrelevance of the periodic potential, continuous translational symmetry is still explicitly broken by it, which leads to true long-ranged translational order in the smectic order parameter $\rho_{\mathbf{G}}$ for $G\hat{\mathbf{y}}$ at multiples of the reciprocal lattice vector $K\hat{\mathbf{y}}$, characterizing the laser potential.

Calculations that closely parallel those of Sec. III A 1 for the FS phase, lead to power-law correlations in the connected part of the translational two-point correlation function

$$C_{\mathbf{G}}^{(c)}(\mathbf{r})\sim\frac{1}{|\mathbf{r}|^{\eta_{\mathrm{FSm}}}}, \tag{3.36}$$

where

$$\eta_{\mathrm{FSm}}=\frac{k_BTG^2}{2\pi\sqrt{B_{xy}B_{yy}}} \tag{3.37}$$

is the exponent characterizing the FSm phase, in analogy to $\overline{\eta}_{\mathbf{G}}$ [Eq. (3.4)], of the FS phase.

The disconnected part of the smectic translational correlation function is finite only at $G=nK$ $(n\in\mathcal{Z})$. The corresponding floating smectic structure function is given by an expression similar to the FS [Eq. (3.12)]. The only difference is that $\overline{\eta}_{\mathbf{G}}$ of the FS phase is replaced by η_{FSm} of the FSm phase and the summation over G is a sum over integer multiples of $2\pi/a$. Consequently, one expects to see sharp peaks only on the q_y axis, with power-law peaks at $G\neq nK$, and true Bragg peaks at $G=nK$. This FSm structure function is schematically displayed in Fig. 15(a).

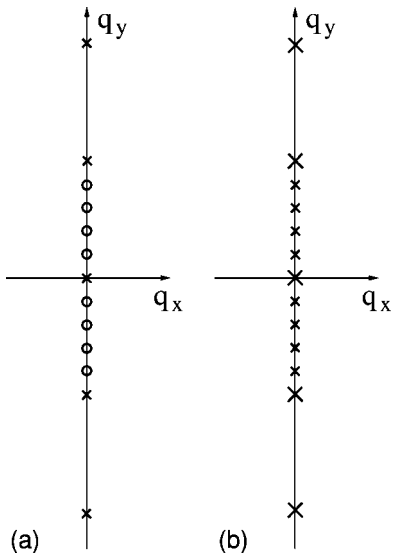

FIG. 15. (a) Schematic of the structure function for the floating smectic phase, characterized by on-q_y-axis quasi-Bragg peaks (open circles) and true Bragg peaks (crosses). (b) Schematic of the structure function for the locked smectic phase, characterized by on-q_y-axis true Bragg peaks, with small and large crosses indicating spontaneously and directly induced translational order.

2. Locked smectic (LSm) phase

As the temperature is lowered, the periodic potential becomes relevant, pinning the smectic layers. The resulting ''locked (LSm) smectic phase'' is characterized by long-range translational order, and, as illustrated in Fig. 15, displays true Bragg peaks at all values of the on-q_y-axis recip-

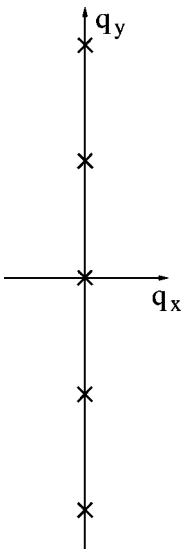

FIG. 16. Schematic of the structure function for the modulated liquid phase, characterized by on-q_y-axis true Bragg peaks located at $n(2\pi/d)$.

rocal lattice vectors $G=n2\pi/a$. At long scales, the effective elastic Hamiltonian that characterizes this phase is simply

$$H_{\mathrm{LSm}}=\frac{1}{2}\frac{\mu}{\xi^2}\int d^2r\, u_y^2, \tag{3.38}$$

with ξ given by Eq. (3.19).

3. Modulated liquid (ML) phase

The modulated liquid phase is the most disordered phase, which occurs at highest temperatures and does not *spontaneously* break any symmetries. It is characterized by a vanishing shear modulus, unbound dislocations, the absence of massless Goldstone modes, and a discrete symmetry of translations along the y axis by a periodic potential constant d. The corresponding structure function of this explicitly orientationally ordered phase, illustrated in Fig. 16, is a set of true Bragg peaks at multiples of the reciprocal lattice vector $K=2\pi/d$ of the periodic potential.

Finite linear translational order parameter susceptibility guarantees that the average order parameter is linear in the strength of the periodic potential. Therefore, as is clear from Eq. (1.17), the strength of the Bragg peaks scales as a *cube* of the input laser intensity, proportional to U_K, as observed in experiments by Clark and co-workers [16,25].

IV. PHASE TRANSITIONS

Phase transitions that take place in our system fall into two broad classes: roughening and melting. However, for high values of the commensurability ratio p $(p>p_c)$ these classes are mathematically related to each other by the duality transformations [42,8], and are both examples of the Kosterlitz-Thouless-type transitions, with kinks and dislocations unbinding, respectively. For $p<p_c$, the roughening transitions are in a different (Ising model and other models with a discrete symmetry) universality class.

A. Roughening transitions

Phase transitions that fall into the roughening transition universality class separate a low temperature ordered phase, in which a potential Goldstone mode is strongly pinned by an external periodic potential, from a quasi-long-range ordered phase, in which the periodic potential is irrelevant in a renormalization group sense. The locked floating solid to floating solid and locked smectic to floating smectic phase transitions, discussed in Sec. III, fall into this broad universality class, although they differ in details that we discuss below.

Despite these small differences the analysis of these transitions are quite similar, and can be done via standard perturbative momentum-shell renormalization group transformation [43,42]. Since smooth (locked) and rough (floating) phases are distinguished by the relevance and irrelevance of the periodic potential, respectively, we can find the transition temperature by analyzing the behavior of $H_{\mathbf{K}}$ [Eq. (2.5)] as a function of length scale. We separate the phonon field, which for a solid phases is a two component vector and a scalar for a smectic, into the high and small wave vector modes,

$$\mathbf{u}(\mathbf{r})=\mathbf{u}^{<}(\mathbf{r})+\mathbf{u}^{>}(\mathbf{r}), \tag{4.1}$$

and integrate the high wave vector part $\mathbf{u}^{>}(\mathbf{r})$ perturbatively in U_K with nonvanishing Fourier components inside a thin momentum shell:

$$\Lambda e^{-l}<|\mathbf{q}|<\Lambda. \tag{4.2}$$

We then rescale the lengths and long wavelength part of the fields with

$$\mathbf{r}=e^{l}\mathbf{r}', \tag{4.3a}$$

$$\mathbf{u}^{<}(\mathbf{r})=e^{\phi l}\mathbf{u}'(\mathbf{r}'), \tag{4.3b}$$

so as to restore the ultraviolet cutoff back to $\Lambda=2\pi/a$. Because the pinning potential nonlinearity is a periodic function, it is convenient (but not necessary) to take the arbitrary field dimension to be

$$\phi=0, \tag{4.4}$$

thereby preserving the period $a=2\pi/\Lambda$ under the renormalization group transformation [44]. Under this transformation the resulting effective Hamiltonian, $H=H_{\mathrm{el}}+H_{\mathbf{K}}$, can be restored into its original form with effective l-dependent elastic and U_K couplings.

For the periodic pinning potential coupling U_K, in a standard way [43,35] we find

$$U_K(l)=U_K e^{2l-(1/2)K_y^2\langle u_y^2\rangle_>}, \tag{4.5}$$

where $\langle u_y^2\rangle_>$ is to be computed with the elastic Hamiltonian appropriate to the phase being analyzed, keeping only modes within an infinitesimal momentum shell near the zone boundary Λ. Hence the nature of the pinning by the substrate

potential and the transition temperature obviously depend on the degree of the translational order in the system, i.e., whether the phase is solid or smectic.

1. Locked floating solid to floating solid phase transition

To determine the critical temperature for the LFS-to-FS phase transition, we compute the $\langle u_y^2\rangle_>$ average using the anisotropic elastic Hamiltonian $H_{\rm el}$ [Eq. (2.25)] describing the 2D solid phase in the presence of a 1D periodic potential. Rewriting $H_{\rm el}$ in terms of Fourier transformed phonon fields $\mathbf{u}(\mathbf{q})$, we find

$$H_{\rm el}=\int \frac{d^2q}{(2\pi)^2}\left[\frac{1}{2}(B_{xx}q_x^2+B_{yx}q_y^2)|u_x(\mathbf{q})|^2 +\frac{1}{2}(K_{xy}q_x^2+K_{yy}q_y^2)|u_y(\mathbf{q})|^2+\delta q_x q_y u_x(\mathbf{q})u_y(-\mathbf{q})\right], \tag{4.6}$$

where

$$B_{xx}\equiv\lambda_{xx}, \tag{4.7a}$$

$$B_{yx}\equiv\mu-\alpha+\gamma, \tag{4.7b}$$

$$K_{yy}\equiv\lambda_{yy}, \tag{4.7c}$$

$$K_{xy}\equiv\mu+\alpha+\gamma, \tag{4.7d}$$

$$\delta\equiv\mu+\lambda_{xy}-\gamma, \tag{4.7e}$$

which, after a simple Gaussian integration, leads to

$$\langle u_y^2\rangle_>=\int_q^> \frac{k_BT}{K_{yy}q_y^2+K_{xy}q_x^2-\dfrac{\delta^2q_x^2q_y^2}{B_{xx}q_x^2+B_{yx}q_y^2}}, \tag{4.8}$$

where we have introduced the shorthand notation $\int_q^> \equiv\int^>[d^2q/(2\pi)^2]$ for the integral over the momentum shell. In the dilute limit, and neglecting effects of the periodic potential on the elastic coefficients, this reduces to

$$\langle u_y^2\rangle_>=\frac{k_BT}{2\pi\bar{\mu}}l, \tag{4.9}$$

with $\bar{\mu}=2\mu(2\mu+\lambda)/(3\mu+\lambda)$. In order to compute $\langle u_y^2\rangle_>$ in general, we use an elliptical (volume conserving) momentum shell defined by major and minor axes $\Lambda_x=\Lambda\sqrt{K_{yy}/K_{xy}}$ and $\Lambda_y=\Lambda\sqrt{K_{xy}/K_{yy}}$. We find

$$\langle u_y^2\rangle_>=\frac{k_BTc_1}{2\pi\sqrt{K_{yy}K_{xy}}}l, \tag{4.10}$$

where we defined a dimensionless number c_1 given by

$$c_1\equiv\int_0^{2\pi}\frac{d\theta}{2\pi}\frac{a_x+(a_y-a_x)\sin^2\theta}{a_x+(a_y-a_x-a_{xy})\sin^2\theta+a_{xy}\sin^4\theta}, \tag{4.11}$$

and

$$a_x\equiv\frac{B_{xx}}{K_{xy}}, \tag{4.12a}$$

$$a_y\equiv\frac{B_{yx}}{K_{yy}}, \tag{4.12b}$$

$$a_{xy}\equiv\frac{\delta^2}{K_{yy}K_{xy}}. \tag{4.12c}$$

Upon combining Eq. (4.10) and (4.5), we find the eigenvalue of the substrate potential to be

$$\lambda_p\equiv2-K_y^2\frac{k_BTc_1}{4\pi\sqrt{K_{yy}K_{xy}}}, \tag{4.13}$$

which, after setting

$$\lambda_p(T_{p\rm S})=0 \tag{4.14}$$

gives us the depinning transition temperature $T_{p\rm S}$

$$k_{\rm B}T_{p\rm S}=\frac{8\pi}{c_1}\sqrt{K_{yy}K_{xy}}\left(\frac{d}{2\pi}\right)^2, \tag{4.15}$$

which separates the LFS and FS phases. In the dilute limit the transition temperature reduces to

$$k_BT_{p\rm S}=8\pi\bar{\mu}\left(\frac{d}{2\pi}\right)^2. \tag{4.16}$$

2. Locked smectic to floating smectic phase transition

As discussed in Sec. III B, at low colloidal densities our system can exhibit LSm and FSm phases, and therefore undergo a phase transition between them in the roughening universality class. Analogously to the LFS-FS phase transition analyzed above, we can calculate the pinning temperature for the LSm-FSm phase transition by computing the $\langle u_y^2\rangle_>$, that goes into Eq. (4.5), and finding the temperature at which this RG eigenvalue vanishes. Using the Hamiltonian $H_{\rm Sm}$, [Eq. (3.35)] appropriate for the smectic phases and computing to zeroth order in the pinning potential U_K, we find

$$\langle u_y^2\rangle_>=\int_q^>\frac{k_BT}{B_{xy}q_x^2+B_{yy}q_y^2} \tag{4.17}$$

$$=\frac{k_BT}{2\pi\sqrt{B_{yy}B_{xy}}}l, \tag{4.18}$$

where for convenience we again used an elliptical momentum shell with axes $\Lambda\sqrt{B_{yy}/B_{xy}}$ and $\Lambda\sqrt{B_{xy}/B_{yy}}$.

After combining this result with Eq. (4.5), we find that translational pinning by the periodic potential is relevant in a floating smectic phase for $T<T_{p\mathrm{Sm}}$, with $T_{p\mathrm{Sm}}$ given by

$$k_B T_{p\mathrm{Sm}} = 8\pi\sqrt{B_{yy}B_{xy}}\left(\frac{d}{2\pi}\right)^2. \tag{4.19}$$

As discussed in more detail in Sec. V, the elastic moduli in Eqs. (4.15) and (4.19) are functions of the strength of the pinning potential U_K, which in turn is proportional to the input laser intensity I_{in}. Hence the resulting functions $T_{p\mathrm{S}}(I_{\mathrm{in}})$ and $T_{p\mathrm{Sm}}(I_{\mathrm{in}})$ in principle determine the LFS-FS and LSm-FSm phase boundaries displayed in Fig. 5 for colloidal densities commensurate with the 1D periodic potential.

B. Dislocation unbinding transitions

In the analysis of Sec. IV A, where we studied a thermal depinning transition within the solid phase, we implicitly assumed that the dislocations that distinguish the 2D solid and smectic phases from the higher temperature disordered phases remain bound. Hence these calculations for the pinning transitions and Eqs. (4.15) and (4.19) remain valid only if they fall below the corresponding dislocation unbinding melting transition temperatures, which we now compute.

1. Locked floating solid to locked smectic phase transition

It is easy to see from the effective Hamiltonian H_{LFS} [Eq. (3.20)] that the most striking consequence of the 1D periodic potential is that it leads to the LFS phase, in which the phonon degree of freedom u_y, corresponding to displacements transverse to the potential troughs acquires a ''mass'' [Eq. (3.19)], and as a consequence is effectively suppressed. Therefore, this phonon mode can be safely integrated out, leaving an effective anisotropic 2D XY Hamiltonian, with temperature and potential strength dependent *effective* elastic constants,

$$H_{\mathrm{LFS}} = \tfrac{1}{2}\int d^2r[B_{yx}(\partial_y u_x)^2 + B_{xx}(\partial_x u_x)^2], \tag{4.20}$$

that describes a locked floating solid at scales longer than the correlation length ξ introduced in Sec. III A 2.

The melting of the LFS phase can be understood in terms of dislocation unbinding. However, in contrast to melting in the absence of an external (e.g., substrate or laser) potential [5], here only the so-called type I dislocation pairs (in the notation of Ref. [37]) with Burgers vectors $\pm\mathbf{b}_1 = \pm b_{\vec{n}}\hat{\mathbf{x}}$ (see Sec. II B) aligned parallel to the trough direction (which we continue to take along the x axis) can be thermally unbound. In the presence of a periodic potential, oppositely charged dislocations, with Burgers vectors not satisfying the above condition (type II dislocations), are bound by a potential which grows linearly with the separation and therefore cannot thermally unbind. This discussion is consistent with the mapping onto *scalar* Coulomb gas Hamiltonian, expected to describe logarithmically bound type I dislocations, embodied in the 2D anisotropic XY model Hamiltonian [Eq. (4.20)].

Away from the dislocation core, for a commensurate orientation defined by the shortest direct lattice vector pointing parallel to the troughs, $\mathbf{R}_{\vec{n}} = n_1\mathbf{e}_1 + n_2\mathbf{e}_2$, labeled by direct lattice Miller indices n_1 and n_2 defined by Eqs. (2.6)–(2.8), the displacement vector $\mathbf{u}$ for the active type I dislocation is given by

$$\mathbf{u} = \hat{\mathbf{x}}\frac{b_{\vec{n}}}{2\pi}\tan^{-1}\left(\frac{yB_{xx}^{1/2}}{xB_{yx}^{1/2}}\right), \tag{4.21}$$

with

$$b_{\vec{n}} = |\mathbf{R}_{\vec{n}}| = a\sqrt{n_1^2 + n_2^2 + n_1 n_2}. \tag{4.22}$$

Melting of the LFS phase via unbinding of these defects is identical to the vortex unbinding transition of an anisotropic 2D XY model. A standard calculation [4,5] leads to the prediction for the LFS phase's melting temperature

$$k_{\mathrm{B}}T_{\mathrm{LFS\text{-}LSm}} = \frac{b_{\vec{n}}^2}{8\pi}\sqrt{B_{xx}B_{yx}}, \tag{4.23}$$

and all other concomitant Kosterlitz-Thouless phenomenology. This implies an exponential growth of the translational correlation length [4]

$$\xi_t \approx a e^{c/|T - T_{\mathrm{LFS\text{-}LSm}}|^{1/2}}, \tag{4.24}$$

with c a nonuniversal parameter, and a *universal* ratio of the jump in the geometric mean of the shear and bulk moduli, $B_{yx}(T^-_{\mathrm{LFS\text{-}LSm}})$ and $B_{xx}(T^-_{\mathrm{LFS\text{-}LSm}})$ to $T_{\mathrm{LFS\text{-}LSm}}$ [45].

The resulting high temperature phase is the LSm phase [46], for low colloidal densities (i.e., high commensurability ratio p), and a modulated liquid for high densities ($p \lesssim 1$; see below), for which the smectic is indistinguishable from a liquid. Because of the unusually strong growth of the translational correlation length ξ_t [Eq. (4.24)], the phenomenology of the LSm-FSm phase transition that we studied in Sec. IV A 2 will be modified for $T \to T^+_{\mathrm{LFS\text{-}LSm}}$ by a long crossover from the crystal to smectic (or liquid) elasticity.

It is important to note the distinction between this anisotropic 2D XY melting of a LFS phase into a LSm phase, and an analogous type I melting mechanism of Ostlund and Halperin for melting of uniaxially anisotropic, but substrate-free 2D solids [37]. In the latter case, thermal fluctuations destabilize the resulting 2D smectic phase by further unbinding type II dislocations, asymptotically converting it into a liquid. Here, because of the pinning potential, type II dislocations [e.g., $\pm\mathbf{b}_{2,3}$ for $\vec{p}=(p,0)$] remain bound by a linear potential. The resulting LSm phase is therefore distinct from the (orientationally ordered) modulated liquid (in which type II dislocations are also unbound), separated from it by a thermodynamically sharp phase transition.

2. Floating solid to floating smectic phase transition

A floating solid phase can melt *continuously* via unbinding of the type I dislocations. However, in contrast to the similar melting of a locked floating solid phase, here the

dislocation unbinding in the displacement u_x proceeds in the presence of another spectator massless phonon mode u_y, which is coupled to it. Consequently, as we will show below, this transition is a *nontrivial* extension of the Kosterlitz-Thouless theory, and, to our knowledge is, heretofore unexplored. Once these type I dislocations unbind the most likely resulting phase is the floating smectic phase [46].

The phenomenology of the FS-FSm melting transition can be most easily analyzed by the following steps. We (i) introduce dislocation degrees of freedom into the elastic Hamiltonian $H_{\rm el}$ [Eq. (2.25)], (ii) perform a duality transformation to convert the resulting Coulomb gas Hamiltonian into a modified sine-Gordon model, and (iii) compute the dislocation unbinding temperature by analyzing the resulting dual model.

To execute these standard steps, it is convenient to first perform the following rescalings of spatial coordinates,

$$x \to x(B_{xx}/B_{yx})^{1/4}, \tag{4.25a}$$

$$y \to y(B_{yx}/B_{xx})^{1/4}, \tag{4.25b}$$

which leads to the Hamiltonian

$$H_{\rm FS}=\frac{1}{2}\int d^2r[K_x(\nabla u_x)^2+c_x(\partial_x u_y)^2+c_y(\partial_y u_y)^2 + 2\lambda_{xy}(\partial_x u_x)(\partial_y u_y)+2(\mu-\gamma)(\partial_x u_y)(\partial_y u_x)], \tag{4.26}$$

where we dropped the prime on the rescaled coordinates, and defined elastic constants

$$K_x \equiv \sqrt{B_{xx}B_{yx}}, \tag{4.27a}$$

$$c_x \equiv K_x K_{xy}/B_{xx}, \tag{4.27b}$$

$$c_y \equiv K_x K_{yy}/B_{yx}. \tag{4.27c}$$

Because in the presence of dislocations the displacement field u_x is a multivalued function, it is essential to distinguish the last two terms in Eq. (4.26). In contrast to conventional elastic theory, where dislocations are bound and u_x is a well-defined function, here these terms *cannot* be transformed into each other by an integration by parts. Keeping track of this distinction ensures the proper form for the elastic constants of the resulting smectic phase.

In this new rescaled coordinate system, a type I dislocation located at the origin, with a Burgers vector $\mathbf{b}=b_{\vec{n}}\hat{\mathbf{x}}$, can be represented by a displacement field

$$\mathbf{u}_s=\hat{\mathbf{x}}\,\frac{b_{\vec{n}}}{2\pi}\tan^{-1}\left(\frac{y}{x}\right). \tag{4.28}$$

However, in contrast to the analysis of the melting of the LS phase above, in the presence of a finite $\partial_y u_y$ deformation, the form of type I dislocation given in Eq. (4.28) does not correspond to a relaxed u_x displacement which minimizes the energy. Consequently, we expect [see Eq. (4.34)] a bilinear coupling between the dislocation density and the u_y distortion. For a finite density of dislocations, we define a singular strain $\mathbf{v}_s \equiv \nabla u_x^s$ due to a dislocation density $b(\mathbf{r})$, with the standard relation

$$\nabla \times \mathbf{v}_s = \hat{\mathbf{e}}_z b(\mathbf{r}), \tag{4.29}$$

$$= \hat{\mathbf{e}}_z \sum_{\mathbf{r}_i} b_{\vec{n}} n_{\mathbf{r}_i} \delta^{(2)}(\mathbf{r}-\mathbf{r}_i), \tag{4.30}$$

$$\equiv \hat{\mathbf{e}}_z b_{\vec{n}} n(\mathbf{r}), \tag{4.31}$$

where $\{n_{\mathbf{r}_i}\}$ are integer dislocation charges. A general solution to the above equation is given (in Fourier space) by

$$\mathbf{v}_s(\mathbf{q}) = \frac{i\mathbf{q}\times\hat{\mathbf{e}}_z}{q^2} b(\mathbf{q}) + i\mathbf{q}\chi(\mathbf{q}), \tag{4.32}$$

where $\chi(\mathbf{q})$ is an arbitrary, single-valued function, which for convenience and without loss of generality we can set to zero. After expressing the gradient of the total displacement field $\mathbf{u}_t$ in terms of the dislocation part $\mathbf{v}_s$ and a single valued phonon field $\mathbf{u}$

$$\nabla u_x^t = \mathbf{v}_s + \nabla u_x, \tag{4.33a}$$

$$\nabla u_y^t = \nabla u_y; \tag{4.33b}$$

inserting this into $H_{\rm FS}$, we obtain a Hamiltonian that includes both the elastic and dislocation degrees of freedom:

$$H_{\rm FSd}=\frac{1}{2}\int \frac{d^2q}{(2\pi)^2}\left\{\frac{2b_{\vec{n}}}{q^2}[\lambda_{xy}q_y^2+(\gamma-\mu)q_x^2]n(\mathbf{q})u_y(-\mathbf{q}) + b_{\vec{n}}^2 K_x \frac{|n(\mathbf{q})|^2}{q^2}\right\} + H_{\rm FS}[\mathbf{u}]. \tag{4.34}$$

After putting the system on the lattice, going to the grand canonical ensemble for dislocations, and adding the dislocation core energy E_c to account for the energy coming from short length scales (not included in the above analysis) the total partition function is given by

$$\mathcal{Z}=\int [d\mathbf{u}]\sum_{\{n_r\}} e^{-H_{\rm FSd}-\sum_r E_c n_r^2}. \tag{4.35}$$

In the above, for convenience, we chose to measure all the energies in units of $k_B T$.

To analyze the dislocation unbinding transition, it is convenient to perform a duality transformation on the above Hamiltonian $H_{\rm FSd}$ [42,8]. To do this we introduce an auxiliary Gaussian field ϕ to decouple the Coulomb interaction between dislocations, and use the Poisson summation formula to perform the summation over the set of lattice integers $\{n_r\}$, obtaining

$$\mathcal{Z}=\int [d\phi][d\mathbf{u}]e^{-H_d}, \tag{4.36}$$

where

$$H_d = \int d^2r \left\{ \frac{K_x^{-1}}{2} |\nabla \phi|^2 - V_V[b_{\vec{n}}(\phi + i\theta)] \right\} + H_{\rm FS}[\mathbf{u}]. \tag{4.37}$$

To obtain H_d [Eq. (4.37)], above, we defined a field $\theta(\mathbf{r})$, whose Fourier transform is given by

$$\theta(\mathbf{q}) = \frac{1}{q^2}[\lambda_{xy} q_y^2 + (\gamma - \mu) q_x^2] u_y(\mathbf{q}), \tag{4.38}$$

and used $V_V(\phi)$ to denote the well-known 2π-periodic Villain potential defined by

$$e^{-V_V(\phi)} = \sum_{n=-\infty}^{\infty} e^{-E_c n^2 + in\phi}. \tag{4.39}$$

At low fugacity (large core energy), this potential reduces to a cosine function, leading to

$$H_d = \int d^2r \left\{ \frac{K_x^{-1}}{2} |\nabla \phi|^2 - g \cos[b_{\vec{n}}(\phi + i\theta)] \right\} + H_{\rm FS}[\mathbf{u}], \tag{4.40}$$

with $g \equiv 2e^{-E_c}$.

Now the dislocation unbinding transition in the original model of the floating solid is determined by the vanishing of the RG eigenvalue of $g(l)$ cosine nonlinearity in this dual model, defined by

$$g(l) = g e^{(2 - \eta_g/2)l}, \tag{4.41}$$

where η_g is determined by

$$\eta_g l = b_{\vec{n}}^2 [\langle \phi^2 \rangle_> - \langle \theta^2 \rangle_>], \tag{4.42}$$

with the right-hand side easily computed from the quadratic part of the dual Hamiltonian H_d [Eq. (4.37)]. Specifically,

$$\langle \phi^2 \rangle_> = K_x \int_> \frac{d^2q}{(2\pi)^2} \frac{1}{q^2} \tag{4.43}$$

$$= \frac{\sqrt{B_{xx} B_{yx}}}{2\pi} l \tag{4.44}$$

and

$$\langle \theta^2 \rangle_> = \int_> \frac{d^2q}{(2\pi)^2} \frac{[\lambda_{xy} q_y^2 + (\gamma - \mu) q_x^2]^2}{q^4} \langle |u_y(\mathbf{q})|^2 \rangle \tag{4.45a}$$

$$= \int_> \frac{d^2q}{(2\pi)^2} \frac{\lambda_{xy}^2 q_y^4 + 2\lambda_{xy}(\gamma - \mu) q_y^2 q_x^2 + (\gamma - \mu)^2 q_x^4}{q^4 [c_x q_x^2 + c_y q_y^2 - \delta^2 q_x^2 q_y^2 / (K_x q^2)]} \tag{4.45b}$$

$$= \frac{\lambda_{xy}^2 c_2 + \lambda_{xy}(\gamma - \mu) c_3 + (\gamma - \mu)^2 c_4}{2\pi \sqrt{K_{yy} K_{xy}}} l \tag{4.45c}$$

where

$$c_2 \equiv \int_0^{2\pi} \frac{d\theta}{2\pi} \frac{a_y^2 \sin^4\theta}{[a_x + (a_y - a_x)\sin^2\theta][a_x + (a_y - a_x - a_{xy})\sin^2\theta + a_{xy}\sin^4\theta]}, \tag{4.46a}$$

$$c_3 \equiv \int_0^{2\pi} \frac{d\theta}{2\pi} \frac{2a_{xy}^2 \cos^2\theta \sin^2\theta}{[a_x + (a_y - a_x)\sin^2\theta][a_x + (a_y - a_x - a_{xy})\sin^2\theta + a_{xy}\sin^4\theta]}, \tag{4.46b}$$

$$c_4 \equiv \int_0^{2\pi} \frac{d\theta}{2\pi} \frac{a_x^2 \cos^4\theta}{[a_x + (a_y - a_x)\sin^2\theta][a_x + (a_y - a_x - a_{xy})\sin^2\theta + a_{xy}\sin^4\theta]}. \tag{4.46c}$$

Upon combining these results, we find that a floating solid phase melts into a floating smectic phase at

$$T_{\text{FS-FSm}} = \frac{b_{\vec{n}}^2}{8\pi} \left(\sqrt{B_{xx} B_{yx}} - \frac{\lambda_{xy}^2 c_2 + \lambda_{xy}(\gamma - \mu) c_3 + (\gamma - \mu)^2 c_4}{\sqrt{K_{yy} K_{xy}}} \right), \tag{4.47}$$

which reduces to the melting temperature $T_{\text{LFS-LSm}}$ [Eq. (4.23)] of the LFS phase in the limit $K_{xy}, K_{yy} \to \infty$, in which the spectator phonon u_y mode is frozen out. Not surprisingly, we find that the extra u_y fluctuations of the FS phase always *suppress* the melting temperature of the FS phase relative to that of the LFS phase, i.e., for all range of parameters, $T_{\text{FS-FSm}} < T_{\text{LFS-LSm}}$.

We now demonstrate that once type I dislocations unbind, the resulting Hamiltonian is that of a floating smectic, described by the Hamiltonian $H_{\rm FSm}$, given in Eq. (3.35). To see this return to the Hamiltonian $H_{\rm FSd}$ [Eq. (4.34)], and note that once dislocations unbind and therefore appear in large densities, the discrete dislocation field $n_{\mathbf{r}}$ can, to a good approximation, be treated as a continuous density $n(\mathbf{r})$. Within this Debye-Hückel approximation the dislocation degrees of freedom can be easily integrated out of the partition function [Eq. (4.35)] by replacing the summation over $n_{\mathbf{r}}$ in $\mathcal{Z}$ by an integration. Simple Gaussian integrations over dislocation

density $n(\mathbf{r})$ and the single valued field u_x then lead, in the long wavelength limit, to an effective floating smectic Hamiltonian

$$H_{\rm Sm}=\frac{1}{2}\int d^2r\{\kappa(\partial_x^2 u_y)^2+B_{xy}(\partial_x u_y)^2+B_{yy}(\partial_y u_y)^2\}, \tag{4.48}$$

where we have restored the original scaling of the spatial coordinates [Eqs. (4.25)], and derived the effective elastic constants for the resulting FSm phase:

$$\kappa=\frac{(\mu-\gamma)^2}{(\mu+\gamma-\alpha)^2}\left(\frac{2E_c}{b_{\vec{n}}^2}\right), \tag{4.49a}$$

$$B_{xy}=\frac{4\mu\gamma-\alpha^2}{\mu+\gamma-\alpha}, \tag{4.49b}$$

$$B_{yy}=\lambda_{yy}-\frac{\lambda_{xy}^2}{\lambda_{xx}}. \tag{4.49c}$$

We note that B_{xy} vanishes as $\gamma,\alpha\to 0$, as it must in this rotationally invariant limit, in which one must recover the rotationally invariant 2D liquid crystal smectic elasticity [39].

Another equivalent but considerably more straightforward way to obtain the smectic Hamiltonian is to note that in the presence of unbound type I dislocations ∇u_x^t [Eq. (4.33a)] contains both the longitudinal and transverse components, and therefore, despite its appearance, it is no longer a conservative vector constrained to be a gradient of a single-valued function. This observation allows us to incorporate unbound type I dislocations into the Hamiltonian $H_{\rm el}$ [Eq. (2.25)], by the replacement

$$\nabla u_x\to\mathbf{v}, \tag{4.50}$$

with $\mathbf{v}$ an arbitrary 2D vector field. Under this substitution $H_{\rm el}$, Eq. (2.25) transforms into

$$H_{\rm FSd}=\int d^2r\left\{\frac{\mu}{2}(\partial_x u_y+v_y)^2+\frac{\lambda_{xx}}{2}v_x^2+\frac{\lambda_{yy}}{2}(\partial_y u_y)^2 +\lambda_{xy}v_x\partial_y u_y+\frac{\alpha}{2}[(\partial_x u_y)^2-v_y^2]+\frac{\gamma}{2}(\partial_x u_y-v_y)^2\right\}. \tag{4.51}$$

After performing a simple Gaussian integration over the two independent components of $\mathbf{v}$, we immediately obtain a Hamiltonian for the floating smectic phase, which in the long wavelength limit agrees in form and with the expressions for the elastic constants B_{xy} and B_{yy}, obtained in Eqs. (4.48) and (4.49).

V. SHAPE OF THE MELTING CURVE

A. Strong pinning limit and reentrant melting

One of the most interesting observations in the colloidal experiments by Wei *et al.* [22], which in fact stimulated our interest in this problem, is the light-induced *reentrant* melting. As we shall explicitly demonstrate, this melting reentrance is a *generic* consequence of short-ranged screened colloidal interactions and thermal fluctuations, and hence should be prevalent in such 2D systems.

To demonstrate the reentrance as a function of laser intensity, we study the shape of the melting curves for the LFS-ML, LFS-LSm, and FS-FSm phase transitions, which we generally denote by $T_m(U_K)$. The common feature of these transitions is that they are all driven by the unbinding of type I dislocations, with $T_m(U_K)$ [see Eqs. (4.23) and (4.47)] at least in part determined by the renormalized values of the bulk modulus B_{xx} for compression along the troughs and the corresponding shear modulus B_{yx}. Our goal then is to determine how these moduli depend on the potential amplitude U_K.

We first note that these melting boundaries $T_m(U_K)$ are constrained by their limiting values

$$T_m(0)=\frac{b_{\vec{n}}^2}{4\pi}\frac{\mu(\mu+\lambda)}{2\mu+\lambda}, \tag{5.1a}$$

$$T_m(\infty)=\frac{b_{\vec{n}}^2}{8\pi}\sqrt{\mu(2\mu+\lambda)}, \tag{5.1b}$$

where $T_m(0)$ is the well-known result in the absence of an external potential [4–6]. In the opposite limit of *infinite* potential strength, $T_m(\infty)$ is given by Eq. (4.23), with $B_{xx}(U_K\to\infty)\approx 2\mu+\lambda$ and $B_{yx}(U_K\to\infty)\approx\mu$. These results follow from comparing $H_{\rm LFS}$ [Eq. (3.20)], with H_0 [Eq. (2.4)], after freezing out the u_y degree of freedom ($u_y=0$) in H_0, as is appropriate in this $U_K\to\infty$ limit. Although in general there is no universal relation between $T_m(0)$ and $T_m(\infty)$, in a dilute colloidal limit, relevant to the experiments of Wei *et al.* [22], the two Lamé coefficients are equal, $\mu\approx\lambda$, and Eqs. (5.1) reduce to

$$T_m^{\rm dil}(0)=\mu\frac{b_{\vec{n}}^2}{6\pi}, \tag{5.2a}$$

$$T_m^{\rm dil}(\infty)=\sqrt{3}\mu\frac{b_{\vec{n}}^2}{8\pi} \tag{5.2b}$$

$$\approx 1.3T_m^{\rm dil}(0). \tag{5.2c}$$

One might have expected that the melting temperature would simply increase monotonically with U_K from $T_m(0)$ to $T_m(\infty)$. However, as we will now show explicitly, the u_y-mode thermal fluctuations, enhanced as the periodic potential is *lowered* from infinity, generically *increase* the melting temperature for $\kappa a\gg 1$. Consequently, the melting

curve $T_m(U_K)$ must have a maximum in this limit, implying reentrant melting for a band of temperatures as a function of the potential amplitude.

The origin of the reentrance effect can be understood on a heursitic level as follows. Clearly, at *small* U_K, we expect that the increase in the strength of the periodic potential suppresses thermal fluctuations in u_y, thereby lowering the entropy of the liquid (or the smectic) state, and therefore making freezing into a lattice free-energetically less costly. This naturally leads to an *increase* of $T_m(U_K)$ with U_K at low laser intensities. However, for potential strengths $U_K \gg k_B T$, this entropic contribution to the free energy becomes unimportant. In this large U_K limit, the behavior of $T_m(U_K)$ is dominated by a different mechanism having to do with the reduction of the elastic constants with increasing U_K and decreasing temperature. To see this, note that the effective shear modulus $B_{yx}(U_K)$ which enters $T_m(U_K)$ [see Eqs. (4.23) and (4.47)], is determined by the screened Coulomb interaction $V(r)=V_0 \exp(-\kappa r)/r$ between colloidal particles in neighboring troughs. In order to find an effective shear modulus for the u_x modes, one needs to integrate out the massive modes corresponding to displacements perpendicular to the troughs of the laser potential. This will be the route taken further below. Heuristically, one should obtain roughly the same result by assuming that the dominant effect comes from the shear modulus B_{xy} and simply averaging the potential over the massive u_y degrees of freedom, which yields

$$B_{yx}(U_K) \sim \langle e^{-\kappa |\mathbf{r}_{n+1}-\mathbf{r}_n|} \rangle_{u_y}, \tag{5.3}$$

where $\mathbf{r}_n$ and $\mathbf{r}_{n+1}$ are positions of nearest neighbor colloidal particles belonging to the nth and $n+1$st Bragg planes, running parallel to the laser potential troughs. This gives to lowest harmonic order in the fluctuations u_y,

$$\begin{aligned} B_{yx}(U_K) &\sim \langle e^{-\kappa a - \kappa [u_y(n+1)-u_y(n)]} \rangle \\ &\sim e^{-\kappa a} e^{\kappa^2 \langle u_y^2 \rangle} \\ &\approx B_{yx}(\infty) e^{c k_B T/U_K}, \end{aligned} \tag{5.4}$$

with c a dimensionless number of order 1. Such a thermal *enhancement* of the effective shear modulus $B_{yx}(U_K)$, which decreases as thermal fluctuations in u_y are suppressed by increasing U_K, is easy to understand: Even though, in the presence of u_y fluctuations colloidal particles in neighboring troughs spend as much time closer together as further apart, because of the concave form of the interaction potential the enhancement of the effective shear modulus is larger from particles being closer together than the corresponding suppression when they are further apart.

The above simple physical argument for reentrance is supported by detailed microscopic lattice calculations in which we compute *both* the effective shear $B_{yx}(U_K)$ and bulk $B_{xx}(U_K)$ moduli. To do this we start with a microscopic model with a screened repulsive Coulomb interaction $V(r)=V_0 \exp(-\kappa r)/r$, where the screening length κ^{-1} is typically much smaller than a, and V_0 depends on the dielectric constant, κ and the sphere radius [22]. Upon integrating out the u_y modes using the screened Coulomb potential to leading order in $k_B T/U_K$, the calculation in Appendix B gives [for orientation $\vec{p}=(1,0)$]

$$B_{yx}(U_K) \approx B_{yx}(\infty) \left\{ 1 + \frac{9(\kappa a)^2}{64\pi^2} \left(1 + \frac{17}{3\kappa a} \right) \frac{k_B T}{p^2 U_K} \right\}, \tag{5.5}$$

$$B_{xx}(U_K) \approx B_{xx}(\infty) \left\{ 1 + \frac{(\kappa a)^2}{64\pi^2} \left(1 - 8v - \frac{23+104v}{3\kappa a} \right) \frac{k_B T}{p^2 U_K} \right\}, \tag{5.6}$$

where $v = V_0 e^{-\kappa a}/k_B T$, $B_{yx}(\infty) = \frac{3}{8} v k_B T \kappa^2$, and $B_{xx}(\infty) = 3\mu$. *Lowering* the potential strength U_K always *increases* the shear modulus, whereas the behavior of the compressional modulus depends on the magnitude of v and κa. When combined with Eq. (4.23), these expressions imply that the melting temperature increases with decreasing U_K for $\kappa a \gtrsim 5.6$ (in Ref. [22], $\kappa a \approx 10$),

$$T_{\text{LFS-LSm}}(U_K) = T^{\infty}_{\text{LFS-LSm}} \left\{ 1 + \frac{5[(\kappa a)^2 - 31]}{64\pi^2} \left(1 + \frac{13}{3\kappa a} \right) \times \frac{k_B T^{\infty}_{\text{LFS-LSm}}}{p^2 U_K} \right\}, \tag{5.7}$$

thus implying reentrant melting for a band of temperatures as a function of potential strength observed in experiments and illustrated in Figs. 2, 4, and 5. Clearly given the dependence of the $T_{\text{FS-FSm}}$ on the elastic moduli [Eq. (4.47)], we expect the FS-FSm phase transition to display reentrance, although quantitative predictions of the size of the reentrant band are much more difficult.

In obtaining Eq. (5.7), we have clearly ignored additional renormalization of the effective elastic constants by phonon nonlinearities and by bound dislocation pairs, which need to be taken into account for a more precise estimate of the phase boundary. Based on the general structure of Kosterlitz-Thouless-like RG flows, the latter renormalizations generically reduce the elastic moduli, and therefore drive the melting temperature down. Since u_y mode fluctuations, and therefore the renormalizations that they induce, are suppressed by the increasing periodic potential, we expect that $T_m(U_K)$ experiences a larger reduction at small U_K than at large U_K. The known values for the potential-free 2D melting and the 2D XY model downward renormalization constrain the extreme $U_K=0$ and $U_K \to \infty$ ends of the melting curve. Furthermore, since thermal downward renormalization of elastic constants is obviously enhanced with increasing temperature, we expect the suppression of the melting temperature due to these effects to be most pronounced near the maximum in $T_m(U_K)$. Clearly, such a U_K-dependent downward renormalization of the elastic constants will generically tend to reduce the range of temperatures over which there is laser-induced reentrant melting. However, these effects are small [47], and we therefore expect reentrant melting to persist even in their presence.

B. Weak pinning: Universal shape of the melting curve at small potential strength

In addition to a maximum displayed by the melting curve as a function of laser intensity, we also find that the shape of the melting temperature is universal in the limit of a vanishing periodic potential strength U_K. This can be seen most easily from the RG scaling theory applied to the potential-free critical point. More specifically, consider the behavior of the translational correlation length $\xi(t,U_K)$ above the melting transition as a function of U_K and the reduced temperature $t \equiv [T - T_m(U_K=0)]/T_m(U_K=0)$. The power of the renormalization group transformation is that it allows us to relate a difficult calculation very close to the transition, where fluctuations are large and perturbation theory is divergent, to a calculation outside of the critical region, where perturbation theory is convergent. Applying this idea to the computation of $\xi(t,U_K)$ we find

$$\xi(t,U_K) = b_* \xi(t(b_*), U_K b_*^{\lambda_K}), \tag{5.8a}$$

$$= e^{c/t^{\bar{\nu}}} \xi(1, U_K e^{c\lambda_K/t^{\bar{\nu}}}), \tag{5.8b}$$

where we have chosen the RG rescaling parameter b_* such that the rescaled reduced temperature $t(b_*)$, given by the RG flow equations of Halperin and Nelson [5], is of order unity:

$$t(b_*) = 1. \tag{5.9}$$

$\lambda_K = 2 - \eta_K/2$ is the renormalization group eigenvalue of the 1D periodic potential U_K. At the primary potential-free fixed point with $U_K = 0$, we recover the well-known [5] exponential growth of the correlation length $\xi(t, U_K = 0)$, with the exponent $\bar{\nu}$ given by

$$\bar{\nu} \approx 0.36963, \tag{5.10}$$

where an overbar denotes critical exponents at this fixed point.

The primary critical behavior is unstable for arbitrarily small U_K. Hence, sufficiently close to the melting temperature $T_m(0)$, the periodic potential always becomes important. This is the case even for the melting of the FS phase, where it leads to a marginal crossover from a fixed line of isotropic rotationally invariant elasticity to the fixed line characterizing elasticity given by Eq. (2.25), where the rotational symmetry is *explicitly* broken by U_K. There, despite the fact that the periodic potential is irrelevant for the translational order parameter, it is always important for the orientational degrees of freedom, since (see Sec. II C) it explicitly breaks orientational symmetry.

In *locked* phases it is clear, from Eq. (5.8b), that for a given small U_K, the effects of this weak periodic potential will be felt at $T_m(U_K) > T_m(0)$, such that the U_K-dependent argument on the right hand side of Eq. (5.8b) is large, i.e., grows beyond order T_m:

$$U_K \approx k_B T_m e^{-c\lambda_K/t_m^{\bar{\nu}}}. \tag{5.11}$$

This then predicts a *universal cusp* for the melting curve $T_m(U_K)$ in the limit $U_K \to 0$ in any phase in which $\lambda_K > 0$, i.e., the periodic potential is relevant and the phase is locked, and $T_m(U_K)$ given by

$$T_m(U_K) \sim T_m(0)\{1 + \lambda_K [\ln(k_B T_m/U_K)]^{-1/\bar{\nu}}\}, \tag{5.12}$$

as depicted in Figs. 2, 4, and 5. For *floating* phases, such as the FS and FSm phases, where the periodic potential is irrelevant (in the RG sense), we expect the convergent perturbation theory in U_K to lead to a melting temperature $T_m(U_K)$ that instead grows *linearly* with U_K.

VI. RESPONSE OF THE TRANSLATION AND HEXATIC ORDER PARAMETER TO AN EXTERNAL POTENTIAL

In this section we use a renormalization group scaling analysis to determine the response of the translational order parameter $M_{\mathbf{K}} = \langle \rho_{\mathbf{K}} \rangle$ and the bond orientational order parameter $\psi_6 = \langle e^{6i\theta(\mathbf{r})} \rangle$ to the amplitude U_K of the external laser potential. In the absence of an external potential, $U_K = 0$, there are only algebraic peaks in the static structure function of the crystalline phase, and the translational order parameter $M_{\mathbf{K}} \equiv \langle \rho_{\mathbf{K}} \rangle$ vanishes like

$$M_{\mathbf{K}} \sim L^{-\bar{\eta}_{\mathbf{K}}/2} \to 0 \tag{6.1}$$

as the system size $L \to \infty$, where

$$\bar{\eta}_{\mathbf{K}} = \frac{k_B T}{4\pi} \frac{3\mu + \lambda}{\mu(2\mu + \lambda)} \mathbf{K}^2 \tag{6.2}$$

is the critical exponent of the potential-free case [5]. For small values of the external potential U_K we can use standard crossover scaling analysis to determine how the translational order parameter depends on the amplitude of the laser potential. We start from the scaling behavior of the free energy density under a renormalization group transformation

$$f(U_K, T) = e^{-2l} f[e^{\lambda_{\mathbf{K}} l} U_K, T(l)], \tag{6.3}$$

where $\lambda_{\mathbf{K}}$ is the renormalization group eigenvalue for the periodic potential, and $T(l)$ is the renormalized temperature which characterizes the crystalline phase. Since in the free energy density the laser potential U_K couples linearly to $\rho_{\mathbf{G}}$, we have

$$M_{\mathbf{K}} = -\frac{\partial}{\partial U_K} f(U_K, T), \tag{6.4}$$

and dimensional analysis tells us that the exponent of the correlation function $\langle \rho_{\mathbf{K}}(\mathbf{r}) \rho_{\mathbf{K}}^{\star}(\mathbf{0}) \rangle \sim r^{-\bar{\eta}_{\mathbf{K}}}$ is related to $\lambda_{\mathbf{K}}$ by

$$\lambda_{\mathbf{K}} = 2 - \tfrac{1}{2}\bar{\eta}_{\mathbf{K}}, \tag{6.5}$$

a result consistent with standard perturbative calculation of $\lambda_{\mathbf{K}}$. Hence we obtain the following scaling relation for the translational order parameter

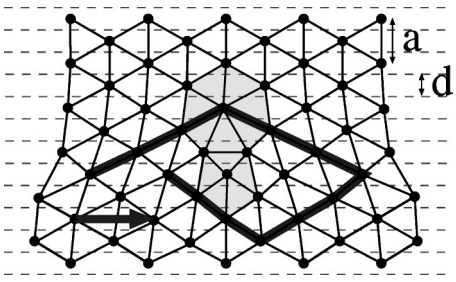

FIG. 17. Triangular lattice with a lattice constant a subject to a periodic potential (maxima indicated by dashed lines) for a dual-primary orientation $\vec{p}=(1,1)$ with $pd=a'$, where $a'=a/2$ is the Bragg plane spacing, and the commensurability ratio is $p=1$. Also shown is the low energy dislocation, with the Burgers vector **b** parallel to the corrugation of the potential.

$$M_{\mathbf{K}}(U_K,T)=e^{-(1/2)\bar{\eta}_{\mathbf{K}}l}M_{\mathbf{K}}[e^{(2-\bar{\eta}_{\mathbf{K}}/2)l}U_K,T(l)], \quad (6.6)$$

where we expect $T(l)$ to approach a finite value as $l\to\infty$. Upon choosing $l=l_*$, such that $e^{(2-\bar{\eta}_{\mathbf{K}}/2)l_*}U_K=\mu a^2$, i.e., is comparable to the elastic energy for deformation at the lattice cutoff a, we obtain

$$M_{\mathbf{K}}(U_K,T)\sim|U_K|^{\bar{\eta}_{\mathbf{K}}/(4-\bar{\eta}_{\mathbf{K}})}. \quad (6.7)$$

For $\bar{\eta}_{\mathbf{K}}>2$, $M_{\mathbf{K}}$ vanishes linearly with U_K, with a singular correction. In contrast, $M_{\mathbf{K}}$ should always vanish *linearly* with U_K in the liquid and hexatic [11,12] phases of the unperturbed colloid.

The laser potential will also induce long-range bond orientational order in $\psi_6=\langle e^{6i\theta(\mathbf{r})}\rangle$ [48]. Along similar lines as above, one can show that the bond order parameter ψ_6 vanishes linearly with U_K in the liquid, vanishes like a power of U_K in the hexatic phase

$$\psi_6\sim|U_K|^{6\bar{\eta}_6/(4-\bar{\eta}_6)}, \quad (6.8)$$

where $\bar{\eta}_6$ is the exponent describing the algebraic decay of bond order, and approaches a nonzero constant as $U_K\to 0$ in the solid phase [26].

VII. DISCUSSION AND EXPERIMENTAL IMPLICATIONS

A. Melting temperatures and critical commensurability ratios in the dilute limit

One of the interesting predictions of our work is that the LFS-ML, LFS-LSm, and FS-FSm phase transitions are all mediated by the unbinding of type I dislocations with Burgers vectors parallel to the troughs of the external potential, $\mathbf{b}=b_{\vec{n}}\hat{\mathbf{x}}$. Consequently, depending on the choice of relative orientation, the periodic potential can be used to supress the unbinding of a set of dislocations that would otherwise unbind in a ''substrate''-free experiments. For example, in the dual-primary orientation shown in Fig. 17, all *six* fundamental Burgers vectors are confined by a linear potential and therefore cannot unbind entropically. It is therefore the unbinding of non-fundamental dislocations with Burgers vector of charge $\sqrt{3}a$, illustrated in Fig. 17, that will control the melting transition.

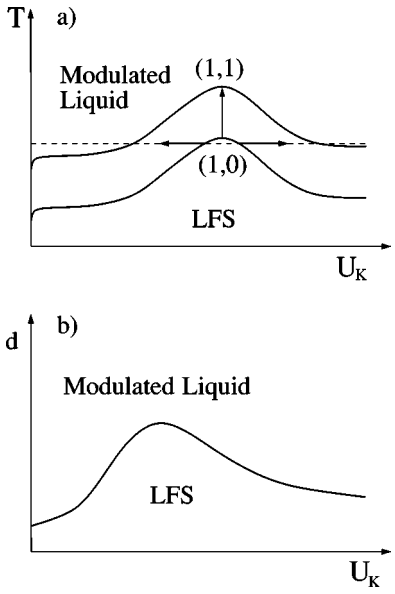

FIG. 18. (a) Schematic $p=1$ phase diagram as a function of potential strength U_K and relative orientation between the laser potential and the 2D solid; a change in orientation from (1,0) to (1,1) is generated by keeping the particle density (and hence the mean particle spacing a) fixed, and varying the distance d between the minima of the external potential. (b) Schematic $p=1$ phase diagram for lattice spacing d vs potential strength U_K at fixed temperature T and fixed colloidal density; incommensurability effects are disregarded.

In general, the magnitude $b_{\vec{n}}^2=a^2(n_1^2+n_2^2+n_1n_2)$ of the lowest energy Burgers vector and hence the melting temperature $T_m\propto b_{\vec{n}}^2$ depends strongly on the relative orientation between the 2D solid and the laser potential, e.g., for $n_2=1$ and $n_1=0$, 1, 2, and 3 one finds $b_{\vec{n}}^2/a^2=1$, 3, 7, and 13. In particular, if one keeps the mean particle spacing a (i.e., the density) and the potential strength fixed and reduces the spacing d between the laser troughs (by, e.g., varying the angle between the two interfering laser beams) $d\to d/\sqrt{3}$ such that one goes from preferred primary lattice orientation $[\vec{n}_A=(1,0)]$ to preferred secondary primary lattice orientation $[\vec{n}_B=(1,1)]$ the melting temperature should increase by a factor of 3 [see the vertical arrow in Fig. 18(a)]. This appears to be consistent with preliminary data of Bechinger *et al.* [49]. They find that for exactly such a change in trough spacing the onset of light induced freezing at *fixed temperature* is shifted to smaller laser intensities also by roughly a factor of 3 [see the horizontal arrow in Fig. 18(a)].

More detailed experimental studies of $T_m(U_K)$ for various commensurate orientations and trough spacings would clearly be desirable in order to systemmatically test our predictions for the orientation dependence of the melting transition temperature for the LIF phase. In performing such studies one must keep in mind considerable irreversibility effects that are expected to plague ''zero-laser-field'' cooled experiments. In order to avoid dealing with long equilibration times, one would need to warm up into the liquid state, change the laser potential period d and only then ''field cool'' back into the solid.

Since trough spacing d (controlled by the angle between the interfering laser beams) and laser intensity appear to be convenient experimentally tunable parameters, it is valuable to derive the shape of the melting curve in the d-U_K plane (for a given temperature and a fixed density of colloidal particles). However, since an arbitrary value of d will in general not be commensurate with the spacing between a particular fixed set of Bragg planes, a detailed study of incommensurate potentials would need to be done in order to fully understand the behavior as a function of trough spacing d. We hope to discuss some of the ensuing physics in a forthcoming publication [27]. However, for the following we would like to restrict ourselves to values of d which are commensurate. Hence, strictly speaking, our results will not be valid for a continuous set of layer spacings but only for a discrete commensurate subset of values. With this precaution in mind we expect the melting curve (for a given temperature and particle density) in the d-U_K plane to have the shape illustrated in Fig. 18(b). We note that in the LIF regime the critical potential strength for melting decreases with decreasing distance between the laser fringes, whereas in the LIM regime the critical potential strength increases as the interference fringes become narrower.

Let us now specialize to the dilute limit $\kappa a \gg 1$, relevant to the experiments of Wei *et al.* [22]. Then the two Lamé coefficients (characterizing the continuum elastic theory of the hexagonal crystal in the absence of a laser potential) become equal, $\mu \approx \lambda$, and the melting temperature for the LFS phase reduces to

$$T_m^0 = \mu \frac{b_{\vec{n}}^2}{6\pi}, \tag{7.1}$$

$$T_m^\infty = \sqrt{3}\mu \frac{b_{\vec{n}}^2}{8\pi} \approx 1.3 T_m^0 \tag{7.2}$$

in the limit of zero and infinite potentials, respectively. For small values of the commensurability ratio, $p < p_c$, the LFS phase melts into a modulated liquid phase or a locked smectic phase. If $p > p_c$, a floating solid phase with two soft phonon modes can intervene between the LFS phase and a modulated liquid or floating smectic phase. As discussed in Sec. IV A, the transition from the LFS into the intermediate FS phase is in a roughening universality class where the laser potential becomes irrelevant. In the dilute limit (and neglecting effects of the periodic potential on the elastic coefficients) the corresponding critical temperature is aproximately

$$T_{p\mathrm{S}}^{\mathrm{dil}} = \frac{3}{\pi}\mu d^2, \tag{7.3}$$

where $d = a'/p$ with $a' = \sqrt{3}a/(2\sqrt{n_1^2 + n_2^2 + n_1 n_2})$ the distance between the Bragg planes parallel to the troughs of the laser potential. Upon combining Eq. (7.3) with Eq. (7.1), the critical commensurability ratio reads

$$p_c^{\mathrm{dil}} = 3\sqrt{\frac{3}{2}} \frac{1}{n_1^2 + n_2^2 + n_1 n_2}. \tag{7.4}$$

Note that only for the primary ($p_c^{\mathrm{dil}} = 3\sqrt{3/2} \approx 3.7$) and dual-primary ($p_c^{\mathrm{dil}} = \sqrt{3/2} \approx 1.2$) orientations is this critical value larger than 1. For any other orientation p_c is less than 1 and hence we expect that there will always be an intervening floating solid phase. A configuration with $\vec{n} = (2,1)$ (also see Fig. 10), and hence $p_c = (3/7)\sqrt{3/2} \approx 0.5$ is likely to be within the range of parameters accessible to experiments with colloidal particles.

For $p > p_c$ there is a roughening transition from a locked floating solid into a uniaxially anisotropic floating solid described by H_{el} [Eq. (2.25)], which subsequently melts (by unbinding of type I dislocations) into either a modulated liquid phase or a floating smectic phase. Since the melting and the roughening transition for a locked smectic phase are given by $T_{m\mathrm{Sm}} = (1/8\pi)Ba^2$ and $T_{p\mathrm{Sm}} = (2/\pi)Bd^2$, respectively, where $B = \sqrt{B_{xy}B_{yy}}$ and a is the smectic layer spacing, there exists a *universal* commensurability ratio $p_c' = 4$ [42] above which a floating smectic phase intervenes between a locked smectic phase or a floating solid phase and the modulated liquid phase. This universal value $p_c' = 4$ should be contrasted with the nonuniversal critical commensurability ratio p_c for the existence of the floating solid phase, which depends on the relative magnitude of the elastic constants and strongly on the relative orientation between the colloidal lattice and the 1D periodic potential. Current experiments find it difficult to access large commensurability ratios p. We hope that our theoretical results will inspire experimentalists to overcome present obstacles and map out the rich phase diagram shown in Fig. 5.

B. Phase diagrams as a function of the Debye screening length

Recent Monte Carlo simulation studies of melting in the presence of a 1D periodic external potential explored the phase diagram in the parameter space of U_K/k_BT and κa with particle density and temperature fixed [19,20]. Although one might question whether such simulations are in equilibrium with respect to dislocation climb (or even glide), it is important to tabulate the predictions of our defect-mediated melting theory in this parameter space in order to be able to compare with the results of these simulations. In addition, it also seems to be more feasable experimentally to map out the phase diagram as a function of potential strength and particle density.

Adapting our results from Sec. V, we find the following behavior. Since the melting temperature is proportional to the elastic moduli, which in turn are proportional to the potential strength, for $\kappa a \gg 1$ we expect T_m to display the following dependence on the screening length $T_m \propto (\kappa a)^2 e^{-\kappa a}$. As an immediate consequence one obtains (in the dilute limit) the following implicit equation [also see Eqs. (7.1) and (7.2)]:

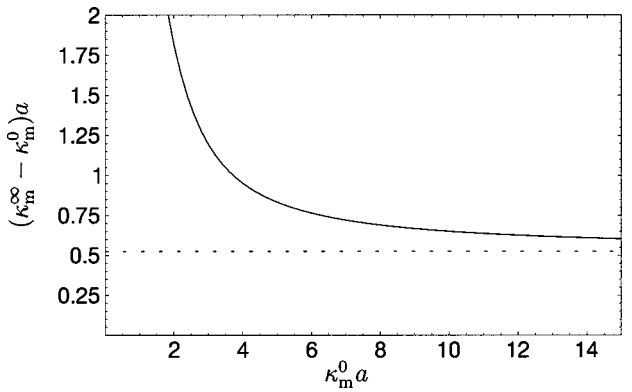

FIG. 19. Difference between $\kappa_m a$ at infinite and zero potential strength as a function of $\kappa_m^0 a$. The vertical dashed line gives the asymptotic value $2\ln 1.3 \approx 0.52$ for very large $\kappa_m^0 a$.

$$(\kappa_m^\infty - \kappa_m^0)a \approx 2\ln\left(1.3\frac{\kappa_m^\infty}{\kappa_m^0}\right) > 0. \tag{7.5}$$

In particular this implies that the difference in the critical values of the inverse screening length at infinite and zero potential strength, κ_m^∞ and κ_m^0, is positive. In the limit $\kappa_m^0 a \gg 1$, Eq. (7.5) reduces to $(\kappa_m^\infty - \kappa_m^0)a \approx 2\ln 1.3 \approx 0.52$. The full solution of Eq. (7.5), together with the asymptotic result, is shown in Fig. 19. We find Eq. 7.5 to be consistent with experimental results [49]. It would be interesting to test experimentally the functional dependence of κ_m^∞ on κ_m^0 (Fig. 19) predicted here.

The results of Monte Carlo simulations appear to disagree with experiments, and with our predictions from the dislocation-mediated melting theory when compared for large values of the potential strength. Whereas we find $\kappa_m^\infty > \kappa_m^0$, the simulations reported in Ref. [19] show quite the opposite. More recent simulations from the same group [20] seem to refute these earlier results and find, in agreement with our theory, $\kappa_m^\infty - \kappa_m^0 > 0$. Their numerical value for $(\kappa_m^\infty - \kappa_m^0)a \approx 1.32$ is, however, more than two times larger than our asymptotic prediction of 0.52. However, because Eq. (7.5) neglects finite renormalization of elastic constants by dislocation dipoles and nonlinear elastic effects, our prediction is an estimate, only accurate upto unknown factors of order 1.

Next we discuss reentrance in the U_K/k_BT-$\kappa_m a$ phase diagram. Upon rewriting Eq. (5.7), we find

$$\frac{U_K}{k_BT} = \frac{\alpha(\kappa_m a)}{T/T_m^\infty(\kappa_m a) - 1}, \tag{7.6}$$

with

$$\alpha(\kappa_m a) = \frac{5[(\kappa_m a)^2 - 31]}{64\pi^2}\left(1 + \frac{13}{3\kappa_m a}\right). \tag{7.7}$$

Hence if $\kappa_m^0 a$ and $\kappa_m^\infty a$ are both smaller than the critical value 5.6 for the existence of reentrance, we expect $(\kappa_m a)^{-1}$ to be a monotonically decreasing function of the potential strength, as shown by the dashed line in Fig. 20. If $\kappa_m^0 a$ and $\kappa_m^\infty a$ are both larger than the critical value 5.6, we expect reentrant behavior such that with increasing potential strength $(\kappa_m a)^{-1}$ first decreases and reaches a minimum $(\kappa_m^{\min} a)^{-1} < (\kappa_m^\infty a)^{-1}$ before it approaches $(\kappa_m^\infty a)^{-1}$ as an inverse power of U_K according to Eq. (7.6) (see Fig. 20). This reentrant behavior is consistent with results from experiments of the Konstanz group [22,49] (see the dashed arrow in Fig. 20, which describes a typical experimental path). It is also similar to what one finds in simulations [19] at small values of the potential strength. However, there are significant differences. First of all, the type of transition is very different. Whereas we discuss a continuous dislocation mediated melting transition, simulations appear to find a first-order transition. Second, as discussed above, the simulations show $\kappa_m^\infty < \kappa_m^0$, which is opposite to what our theory predicts. In more recent simulations [20] $\kappa_m a$ is found to increase monotonically with potential strength with no sign for reentrance. This is opposite to what was found in the earlier simulations by the same group [19].

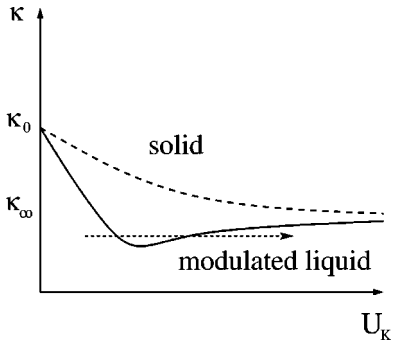

FIG. 20. Schematic $p=1$ phase diagram as a function of potential strength U_K and inverse Debye screening length κ. Solid and dashed curves represent the melting curves for values of κ larger or smaller, respectively, than the critical value of $\kappa_{\rm crit} a \approx 5.6$.

In summary, we find that our theoretical results are consistent with recent experiments and raise strong doubts on the validity of the Monte Carlo results to date on melting in a 1D periodic potential. This latter failure of simulations is not completely surprising given difficulties of numerical methods on even larger systems to resolved the nature of 2D melting even *without* an external potential [21].

C. Static structure factor and pair correlation function

The quantity that is most directly observed in many experiments on colloidal systems and related simulations is the pair correlation function, defined by

$$g(\mathbf{r}) = \frac{V}{N^2}\sum_{ij}{}' \langle \delta[\mathbf{r} - (\mathbf{r}_i - \mathbf{r}_j)]\rangle, \tag{7.8}$$

where the double sum is over N particles but excludes the diagonal terms where $i=j$. It is related to the static structure factor by

$$g(\mathbf{r}) = \frac{1}{N}\int \frac{d^2q}{2\pi} e^{i\mathbf{q}\cdot\mathbf{r}} S(\mathbf{q}). \tag{7.9}$$

Neglecting the smooth part of the structure factor and taking into account only the center column of Bragg peaks and the two neighboring columns of quasi-Bragg peaks with $\eta_{G_{A,x}}(T_m^-)=1/4$ and $\eta_{G_{B,x}}(T_m^-)=1$, respectively, for the pair correlation function one finds

$$g(\mathbf{r})-1=\sum_{\mathbf{G}_1} C_{\mathbf{G}_1}\cos(\mathbf{G}_1\cdot\mathbf{r})+r^{-\eta_{G_{A,x}}}\sum_{\mathbf{G}_A} C_{\mathbf{G}_A}\cos(\mathbf{G}_A\cdot\mathbf{r}) + r^{-\eta_{G_{B,x}}}\sum_{\mathbf{G}_B} C_{\mathbf{G}_B}\cos(\mathbf{G}_B\cdot\mathbf{r}), \tag{7.10}$$

where $\eta_{G_{\alpha,x}}$ are the exponents characteristic for the LFS phase. Note also that according to Eq. (1.13) these exponents only depend on the x component of the reciprocal lattice vector $\mathbf{G}_\alpha$. The amplitudes $C_{\mathbf{G}_\alpha}$ are proportional to the amplitudes of the corresponding Bragg peaks $\mathbf{G}_1=(2\pi/a')\hat{\mathbf{e}}_y$, and quasi-Bragg peaks, $\mathbf{G}_A$ and $\mathbf{G}_B$, with $G_{A,x}=G_x^0=2\pi/a$ and $G_{B,x}=2G_x^0$ [see Eqs. (3.32a) and (3.33b)].

For $\mathbf{r}\|\hat{\mathbf{x}}$, i.e., looking parallel to the minima of the troughs the sum over the Bragg peaks yields a constant. This simply reflects the effect of the laser potential to induce a periodic modulation of the colloidal particle density with a higher density in the minima of the troughs. Note that this trivially implies that the pair correlation function does *not* approach unity as $x\to\infty$ if $g(x)$ is normalized with respect to the mean density. Since the amplitudes for the quasi-Bragg peaks decay as a power law in the strength of the laser potential with an exponent proportional to $\overline{\eta}_{G_y}$ a reasonable approximation for the pair correlation function reads

$$g(x)-1=\text{const}+g_A\cos(G_x^0x)x^{-\eta_{G_{A,x}}}+g_B\cos(2G_x^0x)x^{-\eta_{G_{B,x}}}. \tag{7.11}$$

The relative magnitude of the amplitudes g_A and g_B depends on the strength of the laser potential. Whereas g_B is independent of U_K (note that the leading quasi Bragg-peak contributing to g_B has $G_{B,y}=0$), g_A vanishes as a nontrivial T-dependent power law in U_K for $U_K/\mu a^2\ll 1$ [see Eq. (3.32b)], increasing the weight of the $x^{-\eta_{G_{A,x}}}$ term with increasing potential strength. This prediction should be accessible to experimental verification. Note that the dependence of the amplitude g_A on the potential strength may lead to U_K-dependent effective exponents when one tries to incorrectly fit the experimental data by a single power law. For illustration, Fig. 21 shows $g(x)-1$ for a special case, where const$=0$, $g_A=g_B=1$, $\eta_{G_{A,x}}=\frac{1}{4}$, and $\eta_{G_{B,x}}=1$, and all length are measured in units of a. Due to the superposition of the two harmonics with different power law amplitudes the minima are much broader than the maxima of the structure factor, a feature which appears to be present in the data of Ref. [22].

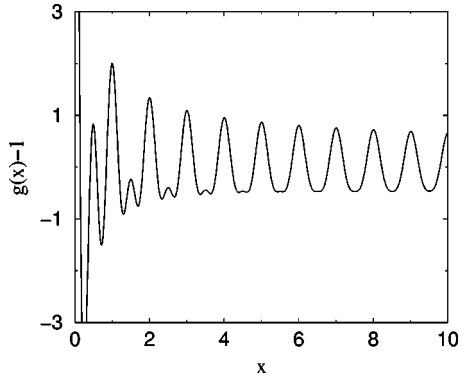

FIG. 21. Algebraic part of the static structure factor for $\mathbf{r}=\hat{\mathbf{x}}$, i.e., looking parallel to the troughs of the laser potential. There are two oscillating contributions, both of which decay algebraically to zero.

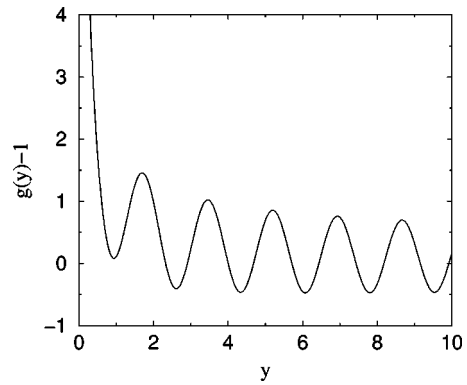

FIG. 22. Algebraic part of the static structure factor for $\mathbf{r}=\hat{\mathbf{y}}$, i.e., looking perpendicular to the troughs of the laser potential. Unlike Fig. 21, algebraically decaying oscillations are superimposed on a periodic contribution (not shown) which does not decay.

For $\mathbf{r}\|\hat{\mathbf{y}}$, i.e., looking perpendicular to the minima of the troughs, we obtain,

$$g(y)-1=\text{const}'\cos(2G_y^0y)+g_A'\cos(G_y^0y)y^{-\eta_{G_{A,x}}}+g_B'y^{-\eta_{G_{B,x}}} \tag{7.12}$$

with $G_y^0=2\pi/\sqrt{3}a$. Hence on top of the periodic density modulation due to the laser potential we again have an algebraic decay from the closest Bragg peaks. For illustration, Fig. 22 shows the algebraic part of the static structure factor $f(x)=y^{-1/4}\cos(2\pi y/\sqrt{3})+y^{-1}$, where we have again chosen the amplitudes to be equal and the η exponents equal to their values at the melting temperature, $\eta_{G_{A,x}}=\frac{1}{4}$ and $\eta_{G_{B,x}}=1$. If one would try to fit the envelope of this function in the regime shown in the graph using a single power law, one would find an exponent of 1/2. Hence caution must be exercised in the analysis of the experimental data, and it is essential to take into account both leading and subleading quasi-Bragg peaks.

ACKNOWLEDGMENTS

It is a pleasure to acknowledge helpful discussions with B. I. Halperin and J. Toner. We also thank C. Bechinger, M. Brunner, and P. Leiderer, and C.-H. Sow and C. M. Murray,

for communicating their unpublished results. L. R. was supported by the NSF through the CAREER Award Grant No. DMR-9625111, University of Colorado's MRSEC Grant No.DMR-9809555 and by the A. P. Sloan and the Packard Foundations. E. F. acknowledges support by the Deutsche Forschungsgemeinschaft through Grant No. SFB 563 and a Heisenberg fellowship (FR 850/3-1). D. R. N. was supported by the NSF through Grant No. DMR97-14725, and Harvard's MRSEC Grant No. DMR98-09363.

APPENDIX A: VARIATIONAL THEORY OF THE 2D MELTING TRANSITION IN THE PRESENCE OF A 1D PERIODIC POTENTIAL

In this appendix we study the freezing transition of the modulated liquid in the limit of a strong periodic potential. In such limit the colloidal particles are tightly confined to the troughs of the 1D periodic potential, and our system reduces to a weakly coupled array of 1D colloidal liquids. The low energy degrees of freedom of the resulting system are then well characterized by a scalar field $u_n(x)$ describing particle displacements along the nth trough and an effective Hamiltonian

$$H=\sum_n \int dx\left\{\frac{1}{2}B\left(\frac{d\phi_n}{dx}\right)^2-g\cos[\phi_{n+1}(x)-\phi_n(x)]\right\}, \tag{A1}$$

where for simplicity of notation we have defined rescaled phonon field $\phi_n(x)$ and elastic couplings B and g related to those defined in Sec. I through

$$\phi_n(x)=\frac{2\pi}{a}u_n(x), \tag{A2a}$$

$$B=Kd\left(\frac{a}{2\pi}\right)^2, \tag{A2b}$$

$$g=\mu d\left(\frac{a}{2\pi d}\right)^2. \tag{A2c}$$

In Sec. I we used simple qualitative arguments to estimate the colloidal freezing transition temperature. Here we would like to treat this model quantitatively and in more detail. Unfortunately, however, as can be seen from a standard renormalization group analysis, *weak* coupling g is always *irrelevant* at long scales, with the effective coupling $g(\xi_x)$ vanishing at length scale ξ_x as

$$g(\xi_x)=g\left(\frac{\xi_x}{a}\right)e^{-\mathrm{const}(k_BT/B)\xi_x}. \tag{A3}$$

Thermal fluctuations, which are especially strong in one dimension, are responsible for this effective decoupling of the colloidal system into effectively independent one-dimensional liquids. This precludes a description of the freezing transition in weak (g) coupling starting from this model. There are two alternatives: One is to study of the melting transition from a complementary strong coupling, fully elastic model with topological defects (dislocations), an approach which lends itself to a rigorous treatment that we undertake in the main part of the paper. Alternatively, an approximate, variational treatment of the model [Eq. (A1)] is possible, and will be presented in this appendix.

The idea behind a variational approach of a problem is that an approximate free energy

$$\tilde{F}=\langle H-H_v\rangle_v+F_v \tag{A4}$$

is an *upper bound* for the exact free energy F corresponding to the Hamiltonian H of interest, and where H_v is *any* other (the so called variational) Hamiltonian, F_v is the corresponding free energy, and the subscript v on the thermal average indicates that a Boltzmann weight with Hamiltonian H_v is used. The advantage of the variational principle can be taken if the arbitrary variational Hamiltonian H_v is judiciously chosen to be simple enough, so that thermal averages can be calculated, but at the same time general enough so as to be able approximately capture the physics of the full Hamiltonian H.

Since, unfortunately, our abilities to compute functional integrals do not extend beyond Gaussians, we choose a quadratic form for H_v,

$$H_v=\sum_n \int dx\left[\frac{B_x}{2}\left(\frac{d\phi_n}{dx}\right)^2+\frac{B_y}{2}(\phi_{n+1}-\phi_n)^2\right], \tag{A5}$$

with B_x and B_y as the effective variational parameters, respectively, related to the effective long wavelength bulk and shear moduli, the latter given by

$$\mu=B_y d\left(\frac{2\pi}{a}\right)^2. \tag{A6}$$

Simple Gaussian averages then lead to the variational free energy density $\tilde{f}(B_x,B_y)=\tilde{F}(B_x,B_y)/L_xN_y$,

$$\tilde{f}=\int_{\mathbf{k}}\left\{\left[\frac{1}{2}(B-B_x)k_x^2-B_y(1-\cos k_y d)\right]G_v(\mathbf{k})-\frac{1}{2}k_BT\log G_v(\mathbf{k})\right\}-g\exp\left[-\int_{\mathbf{k}}(1-\cos k_y d)G_v(\mathbf{k})\right], \tag{A7}$$

where L_x and $N_y(\equiv L_y/d)$ are the length and the number of laser potential troughs (i.e., the 2D dimensions of our colloidal system), respectively, and $G_v(\mathbf{k})$ is the Fourier transform of the intratrough displacement correlation function given by

$$G_v(\mathbf{k})=k_BT[B_xk_x^2+2B_y(1-\cos k_y d)]^{-1}. \tag{A8}$$

To find the upper bound of the free energy density $\tilde{f}$, we now minimize $\tilde{f}(B_x,B_y)$ over the variational parameters B_x and B_y. A conceptually simple but tedious calculation gives

$$B_x=B, \tag{A9a}$$

$$B_y(B,g)=ge^{-k_BT/[\pi d(B_yB)^{1/2}]}. \tag{A9b}$$

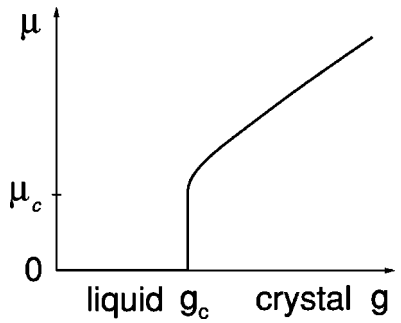

FIG. 23. Shear modulus μ as a function of the intertrough coupling g (at fixed temperature), showing a freezing transition between $\mu=0$ 2D liquid and a $\mu>0$ 2D crystal, and a jump discontinuity at g_c in the shear modulus.

Equation (A9b), which determines the behavior of B_y, and therefore the effective shear modulus μ, as a function of temperature and intertrough coupling g, illustrated in Fig. 23, is the main result of the variational calculation. A simple graphical analysis of Eq. (A9b) predicts

$$B_y(g)=0 \quad \text{for } g<g_c, \tag{A10a}$$

$$B_y(g)\approx g e^{-k_B T/\pi(gB)^{1/2}} \quad \text{for } g\gg g_c, \tag{A10b}$$

where the critical value of the coupling g which separates the two solutions for B_y is given by

$$g_c=\left(\frac{k_B T e}{2\pi}\right)^2 \frac{1}{B}. \tag{A11}$$

Combining this with Eq. (A6), we conclude that the transition between the two solutions in Eq. (A10) represents the freezing of a zero shear modulus ($\mu=0$) 2D liquid into a finite shear modulus ($\mu>0$) 2D solid. In terms of the shear modulus μ and the bulk modulus K, defined by Eqs. (A2c), the corresponding melting transition temperature is given by

$$k_B T_m=\frac{a^2}{2\pi}\sqrt{K\mu}, \tag{A12}$$

a value that, up to factors of order 1, is consistent with the asymptotically exact prediction of our strong coupling (elastic model) analysis given in the main text.

APPENDIX B: EFFECTIVE ELASTIC CONSTANTS FOR SCREENED REPULSIVE COULOMB POTENTIAL

To calculate the effective elastic constants in the limit of large through potential, we start from a model with a pair potential given by a screened repulsive Coulomb potential $V(r)=V_0 a\exp(-\kappa r)/r$, where the screening length κ^{-1} is typically much shorter than the mean particle spacing a. The total potential energy is then given by

$$\Phi=\frac{1}{2}V_0 a\sum_{\langle l,l'\rangle}\frac{1}{|\mathbf{R}_{ll'}|}e^{-\kappa|\mathbf{R}_{ll'}|}, \tag{B1}$$

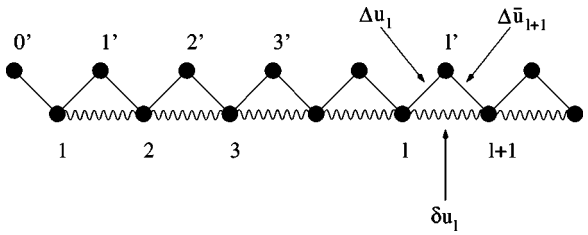

FIG. 24. Sketch of two rows of a triangular lattice of colloidal particles in a trough potential illustrating two contributions to the effective potential energy. The sum over the lattice sites is done by summing along the valleys; there is one intravalley nearest neighbor (wiggly line) and two intervalley nearest neighbors one in the forward direction (Δu) and one in the backward direction ($\Delta\overline{u}$) (solid lines).

where due to the short range of the potential we can safely restrict summation to nearest neighbors, $\langle l,l'\rangle$. The distance between the colloidal particles numbered l and l' can (for a perfect lattice) be decomposed into a distance between the equilibrium positions $\mathbf{r}_l$ and the displacement vectors $\mathbf{u}_l$:

$$\mathbf{R}_{ll'}=\mathbf{r}_l-\mathbf{r}_{l'}+\mathbf{u}_l-\mathbf{u}_{l'}\equiv\mathbf{r}_{ll'}+\mathbf{u}_{ll'}. \tag{B2}$$

In the following we restrict ourselves to the primary configurations, and write the potential energy as sums over Bragg ''planes'' (i.e., rows of particles in $d=2$) indexed by an integer r and particles within these rows indexed by l,

$$\begin{aligned}\Phi=V_0 a\sum_{l,r}\Bigg\{&\frac{1}{[(a+\delta u_l)^2+\delta h_l^2]^{1/2}}\\&\times\exp\{-\kappa[(a+\delta u_l)^2+\delta h_l^2]^{1/2}\}\\&+\frac{1}{[(a/2+\Delta u_l)^2+(d+\Delta h_l)^2]^{1/2}}\\&\times\exp\{-\kappa[(a/2+\Delta u_l)^2+(d+\Delta h_l)^2]^{1/2}\}\\&+\frac{1}{[(a/2+\Delta\overline{u_l})^2+(d+\Delta h_l)^2]^{1/2}}\\&\times\exp\{-\kappa[(a/2+\Delta\overline{u_l})^2+(d+\Delta h_l)^2]^{1/2}\}\Bigg\},\end{aligned} \tag{B3}$$

where the relative intravalley and intervalley displacement fields are defined as follows (see Fig. 24):

$$\delta u_l=u_x(x_l+a,y_l)-u_x(x_l,y_l), \tag{B4}$$

$$\delta h_l=u_y(x_l+a,y_l)-u_y(x_l,y_l), \tag{B5}$$

and

$$\Delta u_l=u_x(x_l+a/2,\,y_l+d)-u_x(x_l,y_l), \tag{B6}$$

$$\Delta\overline{u_l}=-u_x(x_l-a/2,\,y_l)+u_x(x_l,y_l), \tag{B7}$$

$$\Delta h_l=u_y(x_l+a/2,\,y_l+d)-u_y(x_l,y_l). \tag{B8}$$

In the strong pinning limit the laser potential $H_{\mathbf{K}}$ can be expanded in powers of the phonon fields in the y direction,

$$\begin{aligned}\beta H_{\mathbf{K}} &= \frac{U_K}{k_B T} \sum_l \cos\left(\frac{2\pi}{d} h_l\right) \\ &\approx p^2 \frac{8\pi^2}{3} \frac{U_K}{k_B T} \sum_l \left(\frac{h_l}{a}\right)^2 \\ &\equiv k_B T w \sum_l \left(\frac{h_l}{a}\right)^2, \end{aligned} \tag{B9}$$

where we have used $pd=\sqrt{3}a/2$. In the following we shall (in order to simplify notation) measure all lengths in units of the mean lattice spacing.

We proceed as follows: (i) first we expand all terms in the total potential energy Φ to quadratic order in the out-of valley displacement fields; (ii) then we integrate out the massive out-of-valley modes, and (iii) finally we take the continuum limit. Note, that it is only step (i) which explicitly depends on the particular form of the pair potential. For simplicity, we will limit our derivation to the leading order in V_0/U_K and k_BT/U_K.

Step (i) gives

$$\beta\Phi[u,h] = \beta(\Phi_1 + \Phi_2 + \Phi_3), \tag{B10}$$

with

$$\begin{aligned}\Phi_1[u,h] = v \sum_l \{ &-\tfrac{1}{2}(\kappa+1)\delta h_l^2 + \tfrac{1}{2}(\kappa^2+2\kappa+2)\delta u_l^2 \\ &+ \beta_1(\kappa)\delta h_l^2 \delta u_l + \delta_1(\kappa)\delta h_l^2 \delta u_l^2\}, \end{aligned} \tag{B11}$$

$$\begin{aligned}\Phi_2[u,h] = v \sum_l \{ &\tfrac{1}{8}(3\kappa^2+5\kappa+5)\Delta h_l^2 + \tfrac{1}{8}(\kappa^2-\kappa-1)\Delta u_l^2 \\ &+ \alpha_2(\kappa)\Delta h_l \Delta u_l + \beta_2(\kappa)\Delta h_l^2 \Delta u_l \\ &+ \gamma_2(\kappa)\Delta h_l \Delta u_l^2 + \delta_2(\kappa)\Delta h_l^2 \Delta u_l^2\}, \end{aligned} \tag{B12}$$

and $\Phi_3[\overline{u},h]$ obtained from $\Phi_2[u,h]$ by the replacement $\Delta u_l \to \Delta \overline{u}_l$. Here we have also introduced

$$\beta_1(\kappa) = \tfrac{1}{2}(\kappa^2+3\kappa+3), \tag{B13}$$

$$\delta_1(\kappa) = -\tfrac{1}{4}(\kappa^3+5\kappa^2+12\kappa+12) \tag{B14}$$

and

$$\alpha_2(\kappa) = \frac{\sqrt{3}}{4}(\kappa^2+3\kappa+3), \tag{B15}$$

$$\beta_2(\kappa) = -\frac{1}{16}(3\kappa^3+14\kappa^2+33\kappa+33), \tag{B16}$$

$$\gamma_2(\kappa) = -\frac{\sqrt{3}}{16}(\kappa^3+2\kappa^2+3\kappa+3), \tag{B17}$$

$$\delta_1(\kappa) = \tfrac{1}{64}(3\kappa^4+14\kappa^3+55\kappa^2+123\kappa+123). \tag{B18}$$

The dimensionless ratio

$$v \equiv e^{-\kappa}\frac{V_0}{k_B T} \tag{B19}$$

measures the strength of the pair potential relative to a typical thermal energy. Next we integrate out the massive phonon fields h_l with a Boltzmann weight given by the external potential $H_{\mathbf{K}}$,

$$\exp[-\beta H_{\text{eff}}] = \int [dh] \exp\left[-w\sum_l h_l^2 - \beta\Phi[u,h]\right], \tag{B20}$$

where $\int[dh]$ denotes an integration over the $\{h_l\}$. We find

$$\begin{aligned}\beta H_{\text{eff}} = \sum_l \Bigg\{ &\delta u_l^2 \left[\frac{v}{2}(\kappa^2+2\kappa+2) + \frac{v}{w}\delta_1(\kappa) - \frac{v^2}{w}\alpha_2^2(\kappa)\right] \\ &+ (\Delta u_l^2 + \Delta\overline{u}_l^2)\left[\frac{v}{8}(\kappa^2-\kappa-1) + \frac{v}{w}\delta_2(\kappa)\right]\Bigg\}. \end{aligned} \tag{B21}$$

In the continuum limit (and reindroducing the scale a), we have

$$\delta u_l^2 \to a^2(\partial_x u_x)^2, \tag{B22}$$

$$(\Delta u_l^2 + \Delta\overline{u}_l^2) \to a^2\left(\frac{1}{2}(\partial_x u_x)^2 + \frac{3}{2}(\partial_y u_x)^2\right), \tag{B23}$$

$$\sum_l \to \frac{1}{a^2}\int d^2x. \tag{B24}$$

We finally find our desired result, namely,

$$H_{\text{eff}} = \frac{1}{2}\int d^2r[\mu_{\text{eff}}(\partial_y u_x)^2 + K_{\text{eff}}(\partial_x u_x)^2], \tag{B25}$$

with

$$\mu_{\text{eff}} \approx \mu_{\text{eff}}^{\infty}\left\{1 + \frac{9(\kappa a)^2}{64\pi^2}\left(1 + \frac{17}{3\kappa a}\right)\frac{k_B T}{p^2 U_K}\right\}, \tag{B26}$$

$$K_{eff} \approx K_{\text{eff}}^{\infty}\left\{1 + \frac{(\kappa a)^2}{64\pi^2}\left(1 - 8v - \frac{23+104v}{3\kappa a}\right)\frac{k_B T}{p^2 U_K}\right\}, \tag{B27}$$

where

$$\mu_{\text{eff}}^{\infty} = \tfrac{3}{8}((\kappa a)^2 - \kappa a - 1)V_0 e^{-\kappa a}, \tag{B28}$$

$$K_{\text{eff}}^{\infty} = \tfrac{1}{8}(9(\kappa a)^2 + 15\kappa a + 15)V_0 e^{-\kappa a}. \tag{B29}$$

[1] B. I. Halperin, in *Proceedings of the Kyoto Summer Institute 1979—Physics of Low-Dimensional Systems*, edited by Y. Nagaoka and S. Hikami (Publisher, Kyoto, 1979), p. 53.

[2] D. R. Nelson, in *Phase Transitions and Critical Phenomena*, edited by C. Domb and J. L. Lebowitz (Academic, London, 1983), p. 1.

[3] L. D. Landau, Phys. Z. Sowjetunion **II**, 26 (1937); also see S. Alexander and J. McTague, Phys. Rev. Lett. **41**, 702 (1984).

[4] J. M. Kosterlitz and D. J. Thouless, J. Phys. C **6**, 1181 (1973); also see V. L. Berezinskii, Zh. Éksp. Teor. Fiz. **59**, 907 (1970) [Sov. Phys. JETP **32**, 493 (1971)]; **61**, 1144 (1971) [Sov. Phys. JETP **34**, 610 (1972)].

[5] B. I. Halperin and D. R. Nelson, Phys. Rev. Lett. **41**, 121 (1978); D. R. Nelson and B. I. Halperin, Phys. Rev. B **19**, 2457 (1979).

[6] A. P. Young, Phys. Rev. B **19**, 1855 (1979).

[7] R. E. Peierls, Ann. Inst. Henri Poincare **5**, 177 (1935); L. D. Landau, Phys. Z. Sowjetunion **II**, 26 (1937); N. D. Mermin, Phys. Rev. **176**, 250 (1968).

[8] For other examples of sharp phase transitions between disordered phases see, for example, L. Radzihovsky and J. Toner, Phys. Rev. B **60**, 206 (1999); Phys. Rev. Lett. **78**, 4414 (1997); **79**, 4214 (1997), and references therein.

[9] C. C. Huang, in *Bond-Orientational Order in Condensed Matter Systems*, edited by K. J. Strandburg (Springer, New York, 1992).

[10] C. Knobler *et al.*, Annu. Rev. Phys. Chem. **43**, 207 (1992).

[11] C.-A. Murray, W. O. Springer, and R. A. Wenk, Phys. Rev. B **42**, 688 (1990).

[12] K. Zahn, R. Lenke, and G. Maret, Phys. Rev. Lett. **82**, 2721 (1999).

[13] E. Frey, D. R. Nelson, and L. Radzihovsky, Phys. Rev. Lett. **83**, 2977 (1999).

[14] S. N. Coppersmith, D. S. Fisher, B. I. Halperin, P. A. Lee, and W. F. Brinkman, Phys. Rev. B **25**, 349 (1982).

[15] V. L. Pokrovsky *et al.*, in *Solitons*, edited by S. E. Trullinger *et al.* (North-Holland, Amsterdam, 1986), Chap. 3, pp. 71–127.

[16] A. Chowdhury, B. J. Ackerson, and N. A. Clark, Phys. Rev. Lett. **55**, 833 (1985); N. A. Clark, B. J. Ackerson, and A. J. Hurd, *ibid.* **50**, 1459 (1983); B. J. Ackerson and N. A. Clark, Faraday Discuss. Chem. Soc. **76**, 219 (1983).

[17] A. Ashkin and J. M. Dzedic, Appl. Phys. Lett. **19**, 283 (1971); A. Ashkin, Science **210**, 1083 (1980).

[18] J. Chakrabarti, H. R. Krishnamurthy, and A. K. Sood, Phys. Rev. Lett. **73**, 2923 (1994).

[19] J. Chakrabarti, H. R. Krishnamurthy, A. K. Sood, and S. Sengupta, Phys. Rev. Lett. **75**, 2232 (1995).

[20] C. Das, A. K. Sood, and H. R. Krishnamurthy, preprint, cond-mat/9902006.

[21] See, e.g., K. Bagchi, H. C. Andersen, and W. Swope, Phys. Rev. E **53**, 3794 (1996).

[22] Q.-H. Wei, C. Bechinger, D. Rudhardt, and P. Leiderer, Phys. Rev. Lett. **81**, 2606 (1998).

[23] Experiments on colloids, similar to those described in Ref. [11], with a periodic one-dimensional potential provided by lithographic patterning of the confining glass plate, are currently underway at Lucent Technologies [C.-H. Sow and C.M. Murray (private communication)].

[24] K. Lin, J. C. Crocker, V. Prasad, A. Schofield, D. A. Weitz, T. C. Lubensky, and A. G. Yodh, Phys. Rev. Lett. **85**, 1770 (2000).

[25] The scattered intensity $I_{\rm out}$ is clearly proportional to the product of the scattering cross section and the input laser intensity $I_{\rm in}$. Since the former is related to the density-density correlation function, the cross section itself must be proportional to the square of the input laser intensity $I_{\rm in}$, which explicitly induces finite density modulation. Consequently $I_{\rm out} \propto I_{\rm in}^3$.

[26] As explained in detail in Sec. II C, a laser-induced periodic potential, whose strength is proportional to $I_{\rm in}$, induces a nematic ordering field h_{ij} proportional to $I_{\rm in}^2$. The *cube* of the induced nematic order parameter [proportional $(I_{\rm in}^2)^3 = I_{\rm in}^6$] then in turn acts as an ordering field on the hexatic order parameter ψ_6.

[27] E. Frey, L. Radzihovsky, and D. R. Nelson (unpublished).

[28] A set of primary Bragg planes is defined by those parallel planes of colloidal particles within which all particles are related by multiples of a *single fundamental* lattice vector. Equivalently, a set of primary Bragg planes can be defined as those planes, which run perpendicular to one of the *fundamental* reciprocal lattice vectors $\mathbf{G}_i$.

[29] L. S. Levitov, Phys. Rev. Lett. **66**, 224 (1991).

[30] Because an applied periodic potential will generically include the higher harmonics, all of our results for $p=1$ also directly extend to all rational fractions $1/q$, with $q \in Z$.

[31] The factor of $1/d^2$ is inserted into the definition of the discrete model purely for convenience, so as to have the interchannel coupling μ have the same dimensions as the shear modulus $\mu_{\rm eff}$ of the continuum elastic model in Eq. (1.3), which then allows its identification as the microscopic shear modulus.

[32] C. Carraro, Phys. Rev. B **61**, R16 351 (2000); also see M. W. Cole *et al.*, Phys. Rev. Lett. **84**, 3883 (2000).

[33] For $1 < p \leqslant p_c$, our system in principle admits more exotic locked smectic phases, characterized by invariance under discrete translations by nd, where $n \in Z$, but $n \neq p$. Although these phases are thermodynamically distinct, their properties are similar to those that we consider in the main text. We therefore do not study them any further here.

[34] D. J. Bergman and B. I. Halperin, Phys. Rev. B **13**, 2145 (1976).

[35] See, e.g., J. D. Weeks, in *Order in Strongly Fluctuating Condensed Matter Systems*, edited by T. Riste (Plenum, New York, 1980).

[36] Strictly speaking, the elastic Hamiltonian [Eq. (2.4)] is only valid at scales longer than the typical size of a thermally excited dislocation pair, such that the effects of topological defects can be safely incorporated into effective elastic constants μ and λ.

[37] S. Ostlund and B. I. Halperin, Phys. Rev. B **23**, 335 (1981).

[38] It is important to appreciate that even in the FS phase, where the periodic potential is irrelevant in the renormalization group sense, its effects are nontrivial and experimentally observable. For example, in the presence of a periodic potential, even if it is irrelevant, the continuous translational and rotational symmetry is explicitly broken, and the FS phase displays true Bragg peaks in its structure function at multiples of **K**.

[39] P. G. de Gennes, *The Physics of Liquid Crystals* (Oxford University Press, London, 1974); P. G. de Gennes and J. Prost,

The Physics of Liquid Crystals, 2nd ed. (Clarendon Press, Oxford, 1993).

[40] P. Chaikin and T. C. Lubensky, *Principles of Condensed Matter Physics* (Cambridge University Press, Cambridge, 1995).

[41] J. Toner and D. R. Nelson, Phys. Rev. B **23**, 316 (1981).

[42] J. V. José, L. P. Kadanoff, S. Kirkpatrick, and D. R. Nelson, Phys. Rev. B **16**, 1217 (1977).

[43] K. G. Wilson and J. B. Kogut, Phys. Rep. **12C**, 75 (1974).

[44] The choice of the phonon field-rescaling exponent ϕ is of course arbitrary. If instead of the convenient $\phi=0$ choice we left it arbitrary, then to return the Hamiltonian into the form it had before the RG transformation, we would have to also allow the periodic potential wave vector K to flow as $K(l)=Ke^{\phi l}$. In the end the flow equations for the *dimensionless* coupling constants would involve $K(l)$, and would be independent of the choice of ϕ.

[45] D. R. Nelson and J. M. Kosterlitz, Phys. Rev. Lett. **39**, 1201 (1977).

[46] The conclusion of a direct LFS-LSm phase transition is implicitly based on the assumption that the periodic potential that is relevant in the 2D solid phase (LFS) remains relevant (leading to the LSm phase) even when type I dislocation unbind producing a smectic phase. If for a range of parameters $T_{p\mathrm{S}}>T_{\mathrm{pSm}}$ then we would instead expect a direct LFS to *floating* smectic phase transition. Similarly, a direct FS-FSm phase transition may instead be replaced by a direct FS to *locked* smectic phase transition, if $T_{p\mathrm{S}}<T_{\mathrm{pSm}}$ over some parameter range, so that the periodic potential is irrelevant in the 2D solid (FS) phase but becomes relevant in the smectic (LSm) phase, where type I dislocations are unbound. Because of the nontrivial relation between elastic constants in the solid and smectic phases, we cannot exclude the exotic possibilities discussed above based on Eqs. (4.15) and (4.19) for $T_{p\mathrm{S}}$ and T_{pSm}, respectively.

[47] D. S. Fisher, Phys. Rev. B **26**, 5009 (1982): D. S. Fisher, B. I. Halperin, and R. Morf, *ibid.* **20**, 4692 (1979).

[48] See, e.g., L. Balents and D. R. Nelson, Phys. Rev. Lett. **73**, 2618 (1994).

[49] C. Bechinger, M. Brunner, and P. Leiderer (unpublished), and private communication.